~~Aerodynamic response of a floating wind turbine scale model with inclusion of reference control functionalities~~Controller design for model-scale rotors and numerical-experimental study using prescribed motion

Alessandro Fontanella[1], Elio Daka[1], Felipe Novais[1,2], and Marco Belloli[1]

[1]Mechanical Engineering Department, Politecnico di Milano, Milano, Via La Masa 1, 20156, Italy.
[2]Maritime Research Institute Netherlands (MARIN), Wageningen, 6708 PM, the Netherlands.

Correspondence: Alessandro Fontanella (alessandro.fontanella@polimi.it)

Abstract. ~~Design and verification of control strategies for floating wind turbines often makes use of aero-hydro-servo-elastic modeling tools.~~ Aerodynamic loads calculation in ~~these~~ aero-hydro-servo-elastic modeling tools has been recently validated against experiments ~~not including~~ for low-frequency platform motions, but without considering any active wind turbine control capability. This work ~~investigates the aerodynamic response of a floating wind turbine scale model with active control and platform pitch motion. This is done in wind tunnel testing and with modeling of the scaled system in the offshore tool OpenFAST. A control design framework is developed to include the reference wind turbine controller ROSCO in the wind tunnel experiment. With~~ presents a control design framework that to include industry-standard wind turbine control functionalities in a model-scale rotor and its application to a 1:100 scale model of the IEA 15 MW. Wind tunnel tests with fixed foundation and steady wind show the scaled turbine reproduces the steady-state rotor speed-blade pitch-thrust torque characteristics of the IEA 15 MW, confirming the controller design method. Tests with prescribed platform pitch motion ~~, the turbine aerodynamic response is predicted by the numerical model with different accuracy depending on the turbine control regime. Below ratedwind, oscillations of aerodynamic torque in simulations are of lower amplitude than in the experiment, also when dynamic inflow is considered in the aerodynamic model. Above rated wind, where the turbine is controlled with collective blade pitch actuation, the response is not quasi-steady, and differences between the experiment and simulation are larger than in~~ are carried out to assess the turbine response and controller modeling in conditions representative of normal operation of floating wind turbines. The blade element momentum model of OpenFAST is verified against the experiment showing aerodynamic thrust and torque are predicted with higher accuracy in the below-rated ~~wind, in particular for phase with respect to motion.~~ region than above rated: in our simulation, the decrease of thrust oscillations amplitude due to blade pitch actuation is under predicted. This, combined with uncertainty in modeling the blade pitch actuators, complicates the numerical-experimental simulation of the turbine aerodynamic response in above rated operation.

1 Introduction

Floating wind turbine control has been a topic of research since the introduction of floating wind energy. The main reason is the infamous negative damping problem due to the use of the variable-pitch control strategy of bottom-fixed turbines ~~which is discussed, among many, by Larsen and Hanson (2007)and van der Veen et al. (2012)~~(Larsen and Hanson (2007) , van der Veen et al. (2012)). Most of the research in floating wind turbine control tried to devise new control methodologies to ensure stable operation and reduce fatigue loads for the floating wind turbine components.

Design and verification of control strategies often makes use of aero-hydro-servo-elastic modeling tools to assess the response of the floating system~~and predict power production~~. Accuracy of aerodynamic loads calculation in these tools ~~need to be assessed~~ must be validated to ensure correct modeling of the turbine response. ~~This theme~~ The theme of validation of aerodynamic simulation tools for floating wind turbines has recently been the subject the OC6 Phase III project, which addressed the case of large low-frequency platform surge and pitch motion in a scaled wind turbine ~~, whose results are presented by Bergua et al. (2023)and by Cioni et al. (2023). Code validation made use of~~ (Bergua et al. (2023), Cioni et al. (2023)). The OC6 project used data from the wind tunnel experiment of Fontanella et al. (2021) where no active turbine control strategy was ~~used~~considered. The project has shown the aerodynamic response is quasi-static and is correctly captured by codes of different fidelity in case of low-frequency motion and no active turbine control. ~~Additional~~ Instead, additional verification cases run in the OC6 project ~~, has~~ have shown aerodynamic unsteadiness ~~takes~~ may take place when sinusoidal variation of rotor speed or blade pitch is combined with surge motion, but no experimental data were available to ~~verify~~ validate codes in this scenario.

In the last decade, several scale model experiments about the wind-wave response of floating wind turbines have been carried out, and a review of them is presented by Gueydon et al. (2020). The large majority of tests involving a scaled wind turbine and physical wind generation did not use any active turbine control. ~~One example is~~ The research carried out by the DeepCwind consortium, whose results are summarized by Robertson et al. (2013), ~~that~~ investigated the coupled response of three floating wind turbine concepts, but blade pitch and rotor speed were fixed to a constant value ~~as explained by Goupee et al. (2017)~~(Goupee et al. (2017)). Recently, Mendoza et al. (2022) ~~carried out scale model experiments about~~ conducted a scale model experiment of a 15 MW floating wind turbine including active control~~. At~~ , but, at the time of writing, ~~wind-only~~ only preliminary tests with fixed ~~foundation have been examined and~~ tower bottom have been used for the validation of ~~three~~ offshore modeling tools. Another research effort in this topic is the wave basin experiment ~~about~~ of a 10 MW floating wind turbine ~~with active control that were~~ that was carried out by Madsen et al. (2020). Tests with various wind-wave conditions were compared to two offshore codes by Kim et al. (2023) ~~;~~ and the controller used in the simulation study is the same of the experiment. The code validation study of Kim et al. (2023) addressed the floating wind turbine global response, with simultaneous modeling of multiple uncertain phenomena as hydrodynamic viscous loads, turbulent wind field, closed-loop turbine control, rotor aerodynamics with large motion. Overall, the two simulation codes object of ~~the~~ validation showed good accuracy with respect to experimental results. Yu et al. (2017) tested a collective blade-pitch controller system in a wind-wave basin and examined the influence of the turbine controller on the platform global response. A small portion of tests has been modeled with an offshore simulation tool, showing good ~~accuracy~~ agreement for platform motion at the main wave frequency.

However, in the wave-frequency range, platform response is generally driven by linear wave ~~excitation~~ loads and it is difficult to assess the accuracy of aerodynamic loads modeling.

~~The purpose of this work is to investigate the aerodynamic response of a~~ In parallel to experiments with physical modeling of the wind turbine, a large number of floating systems supporting 5 MW-15 MW turbines has been tested in wave basins using a hybrid approach. This approach models rotor loads with a force actuator whose set point is computed in real-time by a numerical model of the full-scale turbine and controller. Gueydon et al. (2018) compared hybrid and physical modeling of wind turbine rotor loads fro a tension leg platform floating wind turbine~~scale model with active control and platform pitch motion. This is done in a wind tunnel experiment and with modeling of the scaled system in the offshore tool OpenFAST. Experiments with active~~ . Thys et al. (2021) investigated the coupling between aerodynamics and hydrodynamics of a 12 MW semi-submersible with a hybrid experiment where aerodynamic loads are computed with a BEM model including the turbine controller and applied to the physical model of the platform and tower with a cable robot. Vittori et al. (2022) tested a 10 MW floating wind turbine reproducing the wind turbine rotor and a state-of-the-art variable-speed control strategy with a multi-fan system. Pires et al. (2020) and Fontanella et al. (2020) utilized the multi-fan system to carry out experiments of the DeepCwind 5 MW and to study the influence on the global floating wind turbine response of two industry-standard control strategies. The hybrid wave basin testing solves the issue related to the downscaling of the controller, but the aerodynamic response of the turbine is reproduced with models that have yet to be validated.

Wind tunnel testing with active control requires control ~~required to develop control~~ tools for the wind turbine scale model~~. There~~ , but there is no consensus or shared practice on how to implement turbine ~~controls~~ controllers in scale model experiments. Often, ~~the controllers utilized in scale model testing~~ controllers of scale model turbines have simplifications with respect to ~~reference controllers used in modeling of~~ those used in utility-scale ~~turbines~~ machines (e.g., the Reference Open Source Controller ROSCO of Abbas et al. (2022b) or the DTU Wind Energy Controller of Meng et al. (2020)). ~~Here, the experiment makes use of the ROSCO, and the same controller of wind tunnel testing is used in simulations. To achieve this goal, a control development framework has been developed and is presented here~~The purpose of this work is to design a closed-loop controller for a scale model wind turbine with an ad-hoc control development framework. The controller has industry-standard functionalities and, once integrated with the aerodynamic design of the scaled rotor, it allows to replicate in the wind tunnel the aerodynamic loads response of a full-scale machine. Wind tunnel experiments are conducted with the controlled scale model to measure the aerodynamic response with fixed foundation and with prescribed low-frequency platform pitch mimicking a floating wind turbine. The turbine of the experiment with its controller are modeled in the offshore simulation tool OpenFAST and simulations are compared to measurements to identify possible sources of uncertainty in the servo-aero-dynamic response of the scaled wind turbine.

The expected impact of this work is to provide ~~information about~~ guidance on how to integrate active wind turbine controls in scale model testing using physical wind. The numerical-experimental study using prescribed platform pitch motion verifies the prediction capability of ~~offshore tools~~ OpenFAST with respect to aerodynamic loading in presence of active turbine control. ~~The methodology we developed to integrate active control in experiments and simulations should benefit future scale model testing activities.~~ Data collected in the experiment, as well as the OpenFAST model of the validation study, are shared with the

Figure 1. Experimental setup in the Polimi wind tunnel. “CS1" and “CS2" are respectively the coordinate systems for platform motion and rotor forces.

community to promote studies about control of floating wind turbines. ~~Data~~ The dataset of the experiment and the OpenFAST model can be used for further validation; the ROSCO controller, which has been implemented in Simulink, can be used in future scale model experiments, but also in control studies for utility-scale turbines.

The structure of this article is as follows. Section 2 describes the wind turbine scale model and the experimental setup of the wind tunnel experiment. Section 3 outlines the wind turbine control strategy and the algorithm we followed to down-scale the controller and implement it in the wind turbine scale model. Section 4 presents the methodology we used to investigate the turbine response and verify the controller design procedure. The article is concluded in Sect. 6.

2 Description of the experimental setup

The experimental setup is shown in Fig. 1. It consists of a wind turbine scale model (WTM), which is mounted on top of a six degrees-of-freedom (DOF) robotic platform. Testing is conducted in the atmospheric boundary layer test section of the Politecnico di Milano wind tunnel, which is 13.84 m wide, 3.84 m high, and 35 m long. The wind turbine is placed 20 m downstream the test section inlet. Tests were performed without roughness elements or turbulence generators for a constant inflow velocity and turbulence intensity of 2%.

2.1 Wind turbine aero-servo-dynamic design

The wind turbine of the experiment is a λ_L = 1:100 scaled version of the IEA 15 MW ~~, presented by Gaertner et al. (2020)~~ (Gaertner et al. (2020)). It was designed to reproduce the aerodynamic response of the full-scale turbine with wind speed reduced by a factor λ_v = 1:3.5~~factor~~.

The aim of rotor aerodynamic design is to replicate the blade normal force of the the IEA 15 MW at design tip speed ratio (TSR) of 9 and blade pitch (β) of 0°. The main difficulty in achieving this goal is Reynolds number, which is 350 times lower than for the full-scale turbine. The blade design uses the SD7032 airfoil, which has suitable lift and lift-to-drag characteristics at Reynolds ~~number lower than 250k that are~~ numbers expected for the turbine ~~model.~~ scale model (i.e., lower than 250k). The blade chord and twist distributions are altered, section by section, to have the lift force and the variation of lift force with angle-of-attack of the IEA 15 MW.

The wind turbine has active generator control and individual blade pitch control. The ~~wind turbine~~ generator is a brushless DC motor *Maxon EC-4pole-30* with planetary gearbox *Maxon GP32HP* of ratio 21. Generator speed is measured with the encoder *ENC 16 EASY* with 500 pulses per turn, and this signal is the main feedback for closed-loop control of the turbine scale model. The generator high-speed shaft is connected to the rotor low-speed shaft with a toothed belt of transmission ratio equal to 2; the total transmission ratio is τ_g = 42 and the transmission efficiency is η_g = 73.5%. The electric motor is driven by a *Maxon ESCON 70/10* controller, it functions as a generator with variable torque ~~setpoint~~ set point, which is computed by the variable-speed control strategy of the turbine controller. The tower is an aluminum tube of 75 mm diameter, and the fore-aft mode is at 9.5 Hz (corresponding to 0.33 Hz full-scale).

The wind turbine has individual blade pitch actuators, housed inside the hub, that are *Harmonic Drive RSF-5B-30-E050-C*. Each pitch actuator is controlled by a *Maxon EPOS 24/2* drive mounted on the turbine hub. Power and blade pitch ~~setpoints~~ set points are transmitted to individual pitch motors with 30 channels slip ring. The wind turbine controller computes generator torque and collective blade pitch ~~setpoints~~ set points for the actuators based on generator speed and wind speed measurements. It runs on a National Instrument PXI embedded control system by means of the Veristand interface.

The main properties of the turbine model are summarized in Table 1.

2.2 Measurements

Quantities measured in the experiment are rotor forces, platform motion, actual generator speed, collective blade pitch ~~setpoint~~set point, hub-height wind speed. Six-component forces at the tower-nacelle interface ~~were~~ are measured with an ATI Mini45 load cell with SI-580-20 calibration. Rotor loads are obtained from the projection in the CS2 reference frame of tower-top loads. Platform pitch motion is measured with two MEL M5L/50 lasers placed beneath the robotic platform. Measurement of the undisturbed wind velocity is obtained with a pitot tube placed at centerline, hub-height, 7.15 m upstream the rotor. Generator speed is measured with the generator encoder and reading of this quantity is an output of the generator drive. Measurement of the actual blade-pitch angle is not available and is replaced with the collective blade pitch ~~setpoint~~set point. All measurements are acquired simultaneously with a NI DAQ with sampling frequency of 2000 Hz.

Table 1. Key parameters of the wind turbine model.

Parameter	Unit	Value
Rotor diameter	m	2.400
Blade length	m	1.110
Hub diameter	m	0.180
Rotor overhang	m	0.139
Tilt angle	°	5.000
Tower-to-shaft	m	0.064
Tower diameter	m	0.075
Tower length	m	1.400
Nacelle mass	kg	1.975
Blade mass	kg	0.240
Rotor mass	kg	2.041
Rotor inertia	kgm^2	0.279
Tower mass	kg	2.190

3 Wind turbine control strategy

The wind turbine controller computes generator torque and collective blade pitch ~~setpoints~~ set points based on generator speed and wind speed measurements. It is uses the algorithms of the ROSCO introduced by Abbas et al. (2022b) and distributed as a DLL and source Fortran code by Abbas et al. (2022a). In this project, the ROSCO has been implemented in MATLAB Simulink, and the same controller implementation is used for the experiment and for co-simulation with OpenFAST.

The logic of the ROSCO ~~used in the experiment~~ implemented in the scaled wind turbine is shown in Fig. 2. It ~~consists of~~ has two main modules~~,~~: a generator torque controller~~that controls generator torque in below-rated wind~~, controlling generator torque below the rated wind speed to achieve maximum wind-power conversion efficiency~~,~~; and a collective blade pitch controller~~that controls aerodynamic torque in above-rated wind~~, controlling aerodynamic torque above the rated wind speed to limit the extracted power to its nominal value. The generator torque and blade pitch controllers are proportional-integral (PI) controllers with this generic structure:

$$y = k_{\mathrm{P},y}(\omega_{\mathrm{g,s}} - \omega_{\mathrm{g}}) + k_{\mathrm{I},y} \int_0^T (\omega_{\mathrm{g,s}} - \omega_{\mathrm{g}}) dt\,, \tag{1}$$

where y is the control input, either generator torque ($y = \mathrm{g}$) ~~of~~ or collective blade pitch ($y = \beta$), $k_{\mathrm{P},y}$ and $k_{\mathrm{I},y}$ are the proportional and integral gains, ω_{g} is generator speed, and $\omega_{\mathrm{g,s}}$ is the generator speed set point.

When wind speed is below rated, blade pitch is held constant to the design value of $0°$, generator torque is controlled to track a constant TSR ~~setpoint~~ set point λ_0 = 9 and to achieve the maximum power coefficient. In scale model testing,

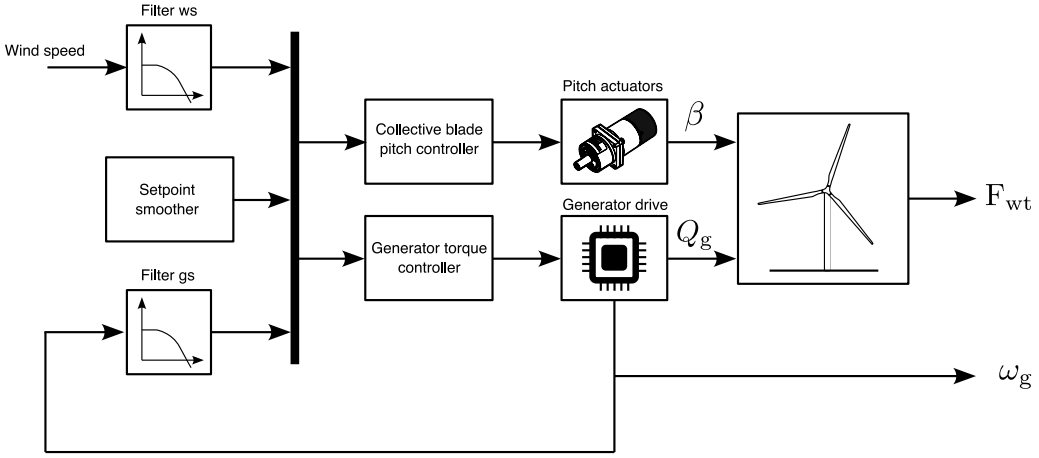

Figure 2. Block diagram showing the ROSCO structure and how it is integrated with the wind turbine scale model. The generator torque controller and collective blade pitch controller are based on the PI controller of Eq. 1, "Filter ws" is the low-pass filter for wind speed, "Filter gs" is the low-pass filter for generator speed, ω_g is the generator speed signal from the generator encoder, $\mathbf{F}_{wt}$ is the 6-components force measured by the tower-top load cell, Q_g is the generator torque, β is the collective blade pitch.

closed-loop TSR tracking is preferred over the more traditional $k\omega^2$ law, also available in ROSCO, because $k\omega^2$ control does not take into account Reynolds-dependency of aerodynamic torque, which occurs in small-scale turbines ~~as it is shown by Fontanella et al. (2023a)~~(Fontanella et al. (2023a)). With TSR tracking:

$$\omega_{g,s} = \tau_g \frac{\lambda_0 \hat{u}}{R}. \tag{2}$$

where R is rotor radius and $\hat{u}$ is the rotor effective wind speed. In general, this is obtained by means of a wind speed estimator, but in this case it is measured with the hub-height pitot tube upstream the turbine model. Generator speed is filtered with a second-order low-pass filter, wind speed with a first-order low-pass filter.

When the turbine is in above-rated operation, generator torque is held constant:

$$Q_g = \frac{P_0}{\eta_g \tau_g \omega_{r,0}}, \tag{3}$$

where P_0 is the turbine rated rotor power, and $\omega_{r,0}$ the rated rotor speed. Collective blade pitch is computed with a PI controller as the one of Eq. 1, where the ~~setpoint~~ set point is $\omega_{g,s} = \tau_g \omega_{r,0}$.

~~In near-rated wind ,~~ When the wind turbine works near the rated wind speed, the set point for the ~~setpoint for~~ generator torque and the collective blade pitch controllers is the same (i.e., ~~the rated speed~~$\omega_{g,s} = \tau_g \omega_{r,0}$). This would lead the controllers to conflict with each other with unwanted oscillations in the turbine response. To avoid this conflict, the ~~setpoint~~ set point smoothing algorithm of Abbas et al. (2022b) is used, that progressively lowers the generator speed ~~setpoint~~ set point of one of the two controllers to have smooth transition between one operating regime to the other. Advanced control functionalities

available in the ROSCO of Abbas et al. (2022a), such as peak shaving or minimum pitch schedule, are implemented in the MATLB Simulink version of the controller but they are not used in ~~the wind tunnel~~ this study.

3.1 ~~Definition~~ Scaling of the wind turbine controller~~parameters~~

In the experiment, the wind turbine controller is run at model scale. This approach takes a different route with respect to ~~the work of Mendoza et al. (2022), where the~~ when the turbine controller is run in real-time in its full-scale version with scaling of input and output signals ~~. The~~ (e.g., in the work of Mendoza et al. (2022)). In Appendix B we prove the full-scale approach does not respect the time ~~scale of the experiment; a proof of this is given in Appendix ??.~~

~~Parameters of the ROSCO are selected to make it fit the WTM scalingand replicate the static and dynamic response of the IEA 15 MW rotor at model scale. Generator speed setpoints of the generator torque and blade pitch controllers are obtained by downscaling values for the IEA 15 MW and introducing the transmission ratio τ_g. The rated generator torque and the rated generator power are defined toachieve the scaled value of rated rotor torque of the reference turbine (see Eq. 3)~~ scaling.

~~Scaling of gains of the PI generator torque and collective blade pitch controllers does not follow dimensional analysis as the rest of the controller parameters, but seeks to downscale the closed-loop~~

The controller scaling seeks to: 1) use the same algorithm of the full-scale turbine controller; 2) replicate the aero-servo-dynamic response of the IEA 15 MW rotor at model scale given the aerodynamic ~~response and drivetrain parameters of the WTM. Tuning the controller to minimize platform motions is outside the scope of this work, and negative damping of platform modes typically found in floating wind turbines is not an issue here since platform motion is prescribed.~~ and structural properties of the wind turbine scale model. The tuning procedure is model-based; dynamics of pitch and generator actuators is neglected. The wind turbine is modeled as a single degree of freedom system corresponding to the rotor-generator, whose equation of motion is:

$$J^*\dot{\omega}_\mathrm{r} = Q_\mathrm{a} - \tau_\mathrm{g}\eta_\mathrm{g}Q_\mathrm{g}\,, \tag{4}$$

where $J^* = J_\mathrm{r} + \eta_\mathrm{g}\tau_\mathrm{g}^2 J_\mathrm{g}$ is the total inertia of the rotor and generator, Q_a the rotor aerodynamic torque. ~~With Eq. 4 a dynamic torque balance is imposed at rotor. This equation is used as a basis for control design, as the objective is to reproduce the aero-servo-dynamic response of the rotor rather than the generator.~~ The aerodynamic torque is:

$$Q_\mathrm{a} = \frac{1}{2}\rho C_Q(\omega_\mathrm{r}, \beta, U)\pi R^3 U^2\,, \tag{5}$$

where ρ is air density and C_Q the torque coefficient. C_Q is assumed to be function of rotor speed, collective blade pitch and wind speed U~~, R is rotor radius~~. The expression of Q_a of Eq. 5 is ~~non linear and is~~ linearized to obtain a linear model of the wind turbine once it is inserted in Eq. 4:

$$Q_\mathrm{a} \simeq Q_{\mathrm{a},0} + \left.\frac{\partial Q_\mathrm{a}}{\partial \omega_\mathrm{r}}\right|_0 (\omega_\mathrm{r} - \omega_{\mathrm{r},0}) + \left.\frac{\partial Q_\mathrm{a}}{\partial \beta}\right|_0 (\beta - \beta_0) + \left.\frac{\partial Q_\mathrm{a}}{\partial U}\right|_0 (U - U_0)\,, \tag{6}$$

where $(\cdot)_0$ denotes the steady-state value of a quantity for a given turbine operating point. In a more compact form:

$$Q_\mathrm{a} \simeq Q_{\mathrm{a},0} + K_{\omega Q}\overline{\omega}_\mathrm{r} + K_{\beta Q}\overline{\beta} + K_{UQ}\overline{U}\,, \tag{7}$$

where $K_{\omega Q}$, $K_{\beta Q}$, K_{UQ} are the aerodynamic torque sensitivities with respect to rotor speed, collective blade pitch and wind speed; $\overline{\omega}_\mathrm{r}$, $\overline{\beta}$, $\overline{U}$ are the perturbations of rotor speed, blade pitch and wind speed.

Below, we detail the scaling of the controller for the below rated and above rated regions.

3.1.1 Below rated

In below-rated operation, blade pitch is fixed ($\overline{\beta} = 0$) ~~,~~ and wind speed is assumed constant ($\overline{U} = 0$)~~and~~ , thus combining Eq. 4 with Eq. 1 we have:

$$J^* \ddot{\overline{\theta}}_\mathrm{r} - (\tau_\mathrm{g}^2 \eta_\mathrm{g} k_{\mathrm{P,g}} + K_{\omega Q}) \dot{\overline{\theta}}_\mathrm{r} - \tau_\mathrm{g}^2 \eta_\mathrm{g} k_{\mathrm{I,g}} \overline{\theta}_\mathrm{r} = 0\,, \tag{8}$$

where θ_r is rotor azimuth. Gains of the TSR tracking controller are computed from Eq. 8~~to have, at model scale, the closed-loop frequency ($\omega_{\mathrm{des},1}$) and damping ($h_{\mathrm{des},1}$) of the IEA 15 MW in below-rated wind:~~ :

$$k_{\mathrm{I,g}} = -\frac{J^*_\mathrm{sm}\, \omega^2_{\mathrm{des},1}}{\tau_\mathrm{g}^2 \eta_\mathrm{g}} \left(\frac{J^* \Omega^2}{\tau_\mathrm{g}^2 \eta_\mathrm{g}} \right)_\mathrm{sm}\,, \tag{9}$$

$$k_{\mathrm{P,g}} = -\frac{K_{\omega Q} + 2 J^*_\mathrm{sm}\, \omega_{\mathrm{des},1}\, h_{\mathrm{des},1}}{\tau_\mathrm{g}^2 \eta_\mathrm{g}} \left(\frac{K_{\omega Q} + 2 J^* \Omega h}{\tau_\mathrm{g}^2 \eta_\mathrm{g}} \right)_\mathrm{sm}\,, \tag{10}$$

where ~~J^*_sm is the rotor-generator inertia of the WTM ,~~ ~~$\omega_{\mathrm{des},1}$~~ $(\cdot)_\mathrm{sm}$ denotes WTM quantities at model scale; Ω = 0.12~~$\lambda_v \lambda_L^{-1}$~~ $\cdot \lambda_u \lambda_L^{-1}$ rad/s, and ~~$h_{\mathrm{des},1}$~~h = 0.85. In ~~general,~~ below-rated wind speeds $K_{\omega Q}$ ~~depends on wind speed, but it~~ is about constant~~in below-rated operation, thus a single~~ , thus we have a single value for $k_{\mathrm{P,g}}$ ~~can be used for any below-rated wind speed~~and $k_{\mathrm{I,g}}$. Gains of the generator torque controller for the WTM are $k_{\mathrm{P,g}} = -8.3 \times 10^{-3}$ Nm/rad/s, instead of -1.1×10^{-1} Nm/rad/s for the scaled IEA 15 MW, and $k_{\mathrm{I,g}} = -1.9 \times 10^{-2}$ Nm/rad instead of -3.7×10^{-1} Nm/rad.

The set point of the TSR tracking controller is computed with Eq. 2.

~~Above rated~~

3.1.2 Above rated

Above the rated wind speed, generator torque is constant ($\overline{Q}_\mathrm{g} = 0$), and assuming ~~again~~ constant wind speed, Eq. 4 becomes:

$$J^* \ddot{\overline{\theta}}_\mathrm{r} + (\tau_\mathrm{g} K_{\beta Q} K_{\mathrm{P},\beta} - K_{\omega Q}) \dot{\overline{\theta}}_\mathrm{r} + \tau_\mathrm{g} K_{\beta Q} K_{\mathrm{I},\beta} \overline{\theta}_\mathrm{r} = 0\,. \tag{11}$$

~~In above-rated wind~~Above rated, aerodynamic sensitivities $K_{\omega Q}$ and $K_{\beta Q}$ depend on wind speed. Gains of the collective pitch controller are computed for discrete wind speeds from rated to cut-out ~~to have for the WTM the same response of the IEA 15 MW. The~~ by means of this procedure:

1. we compute the closed-loop frequency and damping ratio of the IEA 15 MW at wind speed U_0~~are~~:

$$\omega_{\mathrm{des},2}(U_0)\Omega_{0,\mathrm{fs}} = \sqrt{\frac{\tau_\mathrm{g} K_{\beta Q,\mathrm{fs}}(U_0)\, k_{\mathrm{I},\beta,\mathrm{fs}}}{J^*_\mathrm{fs}}} \left(\sqrt{\frac{\tau_\mathrm{g} K_{\beta Q}\, k_{\mathrm{I},\beta}}{J^*}} \right)_{0,\mathrm{fs}}\,, \tag{12}$$

$$h_{\mathrm{des},2}(U_0)_{0,\mathrm{fs}} = \frac{\tau_{\mathrm{g}} K_{\beta Q,\mathrm{fs}}(U_0) k_{\mathrm{P},\beta,\mathrm{fs}} + K_{\omega Q,\mathrm{fs}}(U_0)}{2J^*_{\mathrm{fs}}\,\omega_{\mathrm{des},2}(U_0)} \left(\frac{\tau_{\mathrm{g}} K_{\beta Q} k_{\mathrm{P},\beta} + K_{\omega Q}}{2J^*\Omega} \right)_{0,\mathrm{fs}}, \tag{13}$$

where ~~$(\cdot)_{\mathrm{fs}}$~~ $(\cdot)_{0,\mathrm{fs}}$ denotes full-scale quantities~~. Gains for the WTM at that wind speed are :~~ , that are evaluated at the operating point identified by U_0 in case of wind speed-dependent values;

2. the closed-loop frequency and damping of the WTM are computed by scaling dimensionally those of the IEA 15 MW:

$$k_{\mathrm{I},\beta}(U_0\Omega_{0,\mathrm{sm}} = \Omega_{0,\mathrm{fs}}\cdot\lambda_v) = \frac{J^*_{\mathrm{sm}}\,(\omega_{\mathrm{des},2}(U_0)\,\lambda_v\lambda_L^{-1})^2}{\tau_{\mathrm{g}} K_{\beta Q,\mathrm{sm}}(U_0\lambda_v)}\lambda_L^{-1}, \tag{14}$$

$$k_{\mathrm{P},\beta}(U_0\lambda_v)h_{0,\mathrm{sm}} = \frac{K_{\omega Q,\mathrm{sm}}(U_0\lambda_v) + 2J^*_{\mathrm{sm}}\,(\omega_{\mathrm{des},2}(U_0)\,\lambda_v\lambda_L^{-1})\,h_{\mathrm{des},2}(U_0)}{\tau_{\mathrm{g}} K_{\beta Q,\mathrm{sm}}(U_0\lambda_v)} h_{0,\mathrm{fs}} ; \tag{15}$$

where ~~$(\cdot)_{\mathrm{sm}}$ denotes quantities for the scaled turbine.~~ $(\cdot)_{0,\mathrm{sm}}$ denotes model-scale quantities, that are evaluated at the operating point identified by wind speed $U_0\lambda_v$ in case of wind speed-dependent values.

3. gains for the WTM are:

$$k_{\mathrm{I},\beta}(U_0\lambda_v) = \left(\frac{J^*\Omega^2}{\tau_{\mathrm{g}} K_{\beta Q}} \right)_{0,\mathrm{sm}}, \tag{16}$$

$$k_{\mathrm{P},\beta}(U_0\lambda_v) = \left(\frac{K_{\omega Q} + 2J^*\Omega h}{\tau_{\mathrm{g}} K_{\beta Q}} \right)_{0,\mathrm{sm}}. \tag{17}$$

Equations 16-17 result in the gain schedule for the pitch controller, where the scheduling variable is wind speed. However, since at each wind speed corresponds a steady-state value of collective blade pitch, this is used as the scheduling variable ~~.~~ (i.e., $U_0\lambda_v$ is replaced with β_0). In the WTM there is no feedback of the actual pitch angle and it is replaced with the pitch angle ~~setpoint~~ set point at previous time step.

~~Calculation of gains by means of Eq. 9-10 and Eq. 16-17 requires to compute the aerodynamic sensitivities of the wind turbine at the steady-state operating points. Steady-state conditions of the IEA 15 MW (shown in Fig. 5) were used as a first guess to compute the aerodynamic sensitivities required fro controller tuning based on the $C_P(\lambda,\beta)$ table of the WTM OpenFAST model, and obtain reasonable values of PI gains. Then, with these gains, the WTM OpenFAST model was simulated to obtain a new set of steady-state points, that were used to refine the controller tuning.~~

~~Gains of the generator torque controller for the WTM are $k_{\mathrm{P,g}} = -8.3\times10^{-3}$ Nm/rad/s, instead of -1.1×10^{-1} Nm/rad/s for the scaled IEA 15 MW, and $k_{\mathrm{I,g}} = -1.9\times10^{-2}$ Nm/rad instead of -3.7×10^{-1} Nm/rad.~~ Pitch controller gains for the WTM are compared, at model scale~~with~~ , to those of the IEA 15 MW in Fig.3. Gains for the WTM are significantly different

than values obtained by scaling gains of the IEA 15 MW, the main reason for this difference being rotor inertia, which is larger for the scale model (0.279 kgm^2) compared to the scaled value of the IEA 15 MW (0.031 kgm^2); aerodynamic sensitivities for the WTM are instead close to the reference wind turbine (see Fig. 7). ~~Interestingly, when rotor inertia and aerodynamic sensitivities of the turbine scale model are ideally downscaled the controller tuning procedure isequivalent to scaling the gains of the full-scale turbine.~~

The generator torque set point is computed with Eq. 3, where the generator speed set point is:

$$\omega_{\mathrm{g,s}} = \tau_{\mathrm{g,sm}} \left(\left(\frac{\omega_{\mathrm{g,s}}}{\tau_{\mathrm{g}}} \right)_{\mathrm{fs}} \right) \frac{\lambda_v}{\lambda_L} . \tag{18}$$

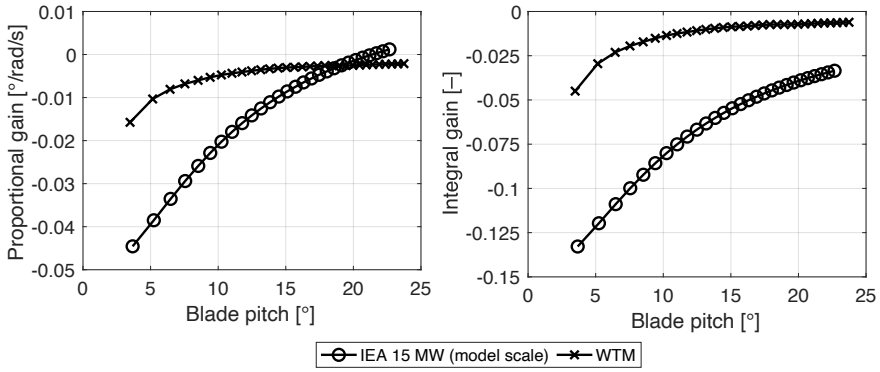

Figure 3. Proportional and integral gains for the collective blade pitch controller of the IEA 15 MW (at model scale) and the wind turbine scale model (WTM) as function of collective blade pitch, which is used for scheduling.

4 Methodology for investigation of the turbine response

~~The wind turbine is subjected to~~ The turbine response and the controller scaling are verified with two sets of tests. The steady-state characteristics of wind speed-rotor speed-blade pitch-thrust-torque are assessed running the wind turbine with steady wind and fixed tower bottom. The aero-servo-dynamic response is studied with prescribed platform pitch motion.

In the experiment, aerodynamic loads are calculated from tower-top load measurements and are compared to two numerical models of the scaled turbine~~, one in OpenFAST and one based on linearized aerodynamics. This~~ :

- an OpenFAST model with generator torque and blade pitch controlled with the ROSCO. This model is used to study the coupled aero-servo-dynamic response of the wind turbine.
- the stand-alone AeroDyn model with prescribed platform pitch motion, rotor speed, and blade pitch. Simulations with this tool are used to assess the aerodynamic loads calculations of the aerodynamic module of OpenFAST without including the additional complexity of the closed-loop turbine controller;

This section summarizes the ~~platform motion conditions~~ operating conditions and the platform motion of the experiment, it explains the algorithm we used to estimate aerodynamic loads from tower-top forces, ~~it~~ and provides a description of the modeling approach adopted in OpenFAST~~, and derives equations of the linearized aerodynamic model~~.

4.1 Wind turbine operating conditions and platform motion

The wind turbine in ~~fixed~~ bottom-fixed configuration is run at several wind speeds ranging from 2.5 m/s to 5.8 m/s to measure the steady-state response of rotor torque and thrust, rotor speed and collective blade pitch.

Two ~~functioning~~ operating conditions are selected for tests with platform motion, corresponding to wind speeds of 2.87 m/s and 5.05 m/s. The imposed motion emulates large-amplitude platform tilt oscillations in floating wind turbines. Motion is in ~~pitch direction~~the pitch direction (θ), i.e., the rotation about the y-axis of the CS1 reference frame (see Fig. 1), and is sinusoidal:

$$\theta(t) = A_\mathrm{m} \sin(2\pi f_\mathrm{m} t)\,, \tag{19}$$

where A_m is motion amplitude and f_m is motion frequency. Rotor-level unsteadiness due to the global response of the rotor and its wake, is often associated to the rotor reduced frequency f_r defined as:

$$f_\mathrm{r} = \frac{f_\mathrm{m} D}{U_0}\,, \tag{20}$$

where D is rotor diameter. Several combinations of A_m and f_m are run in the experiment to explore the turbine aerodynamic response at various f_r and with different amplitude of apparent wind speed oscillations $\Delta U = 2\pi f_\mathrm{m} A_\mathrm{m}$. Motions conditions are summarized in Table 2. Tests with prescribed platform motion are carried out with the turbine controlled by mean of the ROSCO, but also with fixed rotor speed and blade pitch.

4.2 ~~Calculation~~ Estimation of rotor aerodynamic loads

~~Aerodynamic rotor~~ A measurement of aerodynamic loads is not available in the experiment, thus aerodynamic thrust and torque are ~~obtained~~ estimated from measurements of tower-top ~~interface forces. Measurements~~ loads, which are processed to remove the force contribution due to inertia and weight of the rotor-nacelle assembly~~, which is subjected to an acceleration when platform moves~~. For every motion condition, two tests are run where the same type of motion (amplitude and frequency) is prescribed to the wind turbine; in one test there is no wind, the rotor is fixed, and loads measured by the load cell are mostly due to inertia ~~(i.e.,~~ and weight (we assume the contribution due to air drag on the turbine components is negligible); in the test with wind, the load cell measures inertia, weight, and aerodynamic forces. Time series acquired in the two tests are ~~windowed~~ grouped so they have the same integer number of motion periods; time series of forces in the test with no wind are subtracted from time series of forces in the test with wind, after being projected from CS1 to CS2~~.~~, obtaining the aerodynamic loads. This procedure for estimating aerodynamic forces is reliable when dynamic amplification due to flexibility is negligible (Fontanella et al. (2021)), i.e., when the frequency of motion is significantly lower than the first flexible mode of the wind turbine (in our case it is the fore-aft mode at 9.5 Hz and the maximum f_m is 2 Hz).

Table 2. Motion conditions (A_m is amplitude of pitch motion, f_m is frequency, ΔU is the apparent wind speed at hub-height, f_r BR is the reduced frequency with below rated wind of 2.87 m/s, f_r AR the reduced frequency with above rated wind of 5.05 m/s).

A_m [°]	f_m [Hz]	ΔU [m/s]	f_r BR [−]	f_r AR [−]
3.2	0.25	0.13	0.21	0.12
2.2	0.25	0.09	0.21	0.12
1.1	0.25	0.04	0.21	0.12
3.3	0.75	0.40	0.63	0.36
2.2	0.75	0.26	0.63	0.36
1.1	0.75	0.13	0.63	0.36
2.2	1.25	0.45	1.05	0.59
1.7	1.25	0.34	1.05	0.59
1.1	1.25	0.22	1.05	0.59
2.0	1.50	0.48	1.25	0.71
1.7	1.50	0.41	1.25	0.71
1.1	1.50	0.27	1.25	0.71
1.1	1.75	0.31	1.46	0.83
0.8	1.75	0.23	1.46	0.83
0.5	1.75	0.15	1.46	0.83
0.8	2.00	0.27	1.67	0.95
0.5	2.00	0.18	1.67	0.95
0.2	2.00	0.07	1.67	0.95

Rotor speed is regulated by the wind turbine controller and in general, when the turbine operates in unsteady conditions, rotor speed is not constant~~. The~~ , and the inertia torque due to rotor acceleration is present in the load cell measurements. With sinusoidal platform motion, rotor speed oscillations are dominated by the harmonic component at the motion frequency, as it is shown in Fig. 4. Rotor speed oscillations at frequencies other than ~~f_m~~ f_m are regarded as noise. Aerodynamic torque is computed removing the torque component due to rotor inertia from M_x of CS2:

$$Q(t) = M_x(t) - J_\mathrm{r} A_\omega (2\pi f_\mathrm{m})^2 \cos(2\pi f_\mathrm{m} t + \phi_\omega)\,, \tag{21}$$

where A_ω and ϕ_ω are the amplitude and phase of the rotor speed spectrum.

4.3 OpenFAST model

An aero-servo-elastic model of the wind turbine scale model of the experiment is created in OpenFAST~~(v3.1.0). The wind turbine is simulated at full-scale. This is done to avoid the use of small time steps, and because mapping of aerodynamic loads to the structural module of OpenFAST has been shown to be inaccurate with small amplitude forces of scale model rotors~~

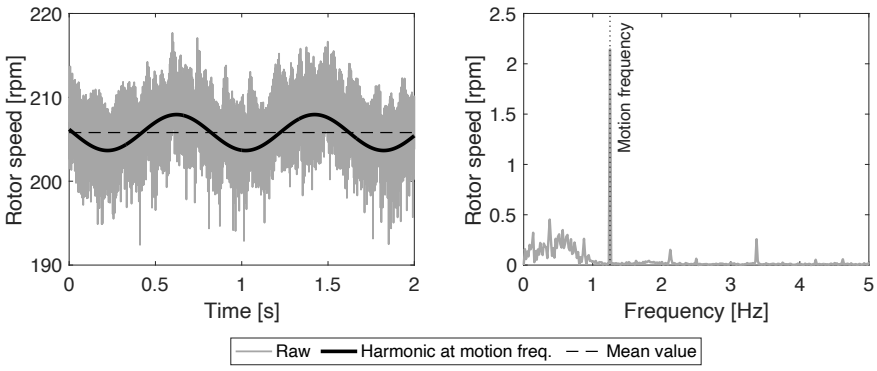

Figure 4. Rotor speed with prescribed platform pitch motion of f_m = 1.25 Hz, A_m = 2.2°. Left: time series, right: spectrum.

~~(forces for the wind turbine scale model are 122500 time smaller than for the IEA 15 MW). Accuracy of this mapping is needed to simulate the wind turbine controller.~~ . Blades and tower are modeled as rigid bodies. A damped oscillator is introduced at the base of the wind turbine and external forces are applied to it to prescribe the platform motion ~~recorded in~~ of the experiment. The aerodynamic model is implemented in ~~AeroDyn15~~ AeroDyn v15 based on blade twist and chord radial distributions, and Reynolds-dependent polars at ~~39~~ 38 radial stations. Calculation of induced velocity in the ~~BEM model of AeroDyn can be~~ AeroDyn BEM is based on wake equilibrium assumption (steady BEM~~, SB~~) or on dynamic wake (dynamic BEM~~, DB); the airfoil model can be based on static polars (SA), or account~~). The airfoil model accounts for flow hysteresis during attached flow and dynamic stall~~(unsteady airfoil, UA). Four combinations of these modeling approaches are considered for simulation of the experiment.~~ .

The wind turbine controller is the same Simulink controller of the experiment which is run in co-simulation with ~~the OpenFASTmodel. Parameters are upscaled from those used in scaled testing by means of dimensional analysis to be consistent with the rest of the OpenFAST model.~~ OpenFAST. Pitch actuators are modeled as third-order systems of transfer function:

$$G_\mathrm{act}(s) = \frac{b_1 s^2 + b_2 s + b_3}{a_1 s^3 + a_2 s^2 + a_3 s + a_4}\,. \tag{22}$$

Coefficients of $G_\mathrm{act}(s)$ are obtained by means of system identification carried out on the WTM before wind tunnel testing. In the frequency range of imposed motion tests, $G_\mathrm{act}(s)$ introduces a constant time delay of 0.075 s (i.e., phase is linear with frequency) and unit amplification.

4.4 ~~Linearized model of rotor aerodynamic loads~~

~~Aerodynamic rotor thrust is written with the same formulation used for torque in Eq. 5 as:~~

$$T = \frac{1}{2}\rho C_T(\omega_\mathrm{r}, \beta, U)\pi R^2 U^2\,,$$

where C_T is the thrust coefficient. Equation **??** is linearized with the same approach used for Eq. 5 and becomes:

$$T \simeq T_0 + K_{\omega T}\overline{\omega_\mathrm{r}} + K_{\beta,T}\overline{\beta} + K_{UQ}\overline{U}\,.$$

In case of a floating wind turbine and steady wind, $\overline{U} = -\dot{x}_\mathrm{hub}$ is the apparent wind speed for the rotor due to rigid-body platform motion, where $\dot{x}_\mathrm{hub}$ is the hub velocity normal to the rotor plane. Equations **??**-6 become:

$$T \simeq T_0 + K_{\omega T}\overline{\omega_r} + K_{\beta T}\overline{\beta} - K_{UT}\dot{x}_\mathrm{h}\,,$$

$$Q \simeq Q_0 + K_{\omega Q}\overline{\omega_r} + K_{\beta Q}\overline{\beta} - K_{UQ}\dot{x}_\mathrm{h}\,.$$

The linearized model of Eq. **??-??** is used to verify if the aerodynamic response with platform pitch motion and active control follows the quasi-steady theory. If quasi-steady theory is valid, the total variation of aerodynamic loads is the sum of variations induced by apparent wind , rotor speed and blade pitch oscillations. With this assumption, the thrust and torque oscillations due to apparent wind is computed from total aerodynamic loads as:

$$\Delta T = (F_x - T_0) - (K_{\omega T}\overline{\omega_r} + K_{\beta T}\overline{\beta})\,,$$

$$\Delta Q = (Q - Q_0) - (K_{\omega Q}\overline{\omega_r} + K_{\beta Q}\overline{\beta})\,,$$

where F_x and M_x are the aerodynamic force and torque in the x-axis of CS2, respectively, and obtained with the algorithm of Sect. 4.2. Platform pitch motion results in rotor speed oscillations and blade pitch actuations with the same frequency of motion:

$$\overline{\omega_\mathrm{r}}(t) = A_\omega \cos(2\pi f_\mathrm{m} t + \phi_\omega)\,,$$

$$\overline{\beta}(t) = A_\beta \cos(2\pi f_\mathrm{m} t + \phi_\beta)\,,$$

where A_β and ϕ_β are the amplitude and phase of the spectrum of blade pitch β, evaluated at frequency equal to f_m. For OpenFAST results, β is the actual value of blade pitch available among simulation outputs; for experimental results β is obtained from the convolution of the collective blade pitch setpoint and the pitch actuator transfer function of Eq. 22. With harmonic motion, the variation of thrust force and torque due to apparent wind is:

$$\Delta T(t) = -K_{UT}(2\pi f_\mathrm{m}) A_\mathrm{hub} \cos(2\pi f_\mathrm{m} t)\,,$$

$$\Delta Q(t) = -K_{UQ}(2\pi f_\mathrm{m}) A_\mathrm{hub} \cos(2\pi f_\mathrm{m} t)\,,$$

with $A_\mathrm{hub} = A_\mathrm{m} d_\mathrm{hub}$, where d_hub is the hub distance from the center of platform pitch rotation (d_hub = 1.48 m, see Fig. 1). When the turbine aerodynamic response is described by Eq. **??-??**, the phase of the force response with respect to motion is $-\pi/2$, and the zero-peak amplitude normalized by amplitude of hub motionis linear with motion frequency:

$$\Delta T / A_\mathrm{hub} = 2\pi f_\mathrm{m} K_{UT}\,,$$

$$\Delta Q / A_\mathrm{hub} = 2\pi f_\mathrm{m} K_{UQ}\,.$$

5 Results

This section presents results about the wind turbine response from experimental measurements and OpenFAST simulations. First, This section presents results about the wind turbine response from experimental measurements and numerical simulations. Experiment and simulation are compared to identify differences in the modeling of the servo-aero-dynamic response of the wind turbine. The results section is organized in this way:

- we verify the steady-state response of rotor speed-blade pitch-thrust-torque characteristics with fixed turbine controlled with the ROSCO are presented. Next, the rotor performance coefficients obtained with steady wind and several combinations of fixed TSR-blade pitch are discussed and utilized to compute the sensitivities of the linearized of the turbine controlled with the ROSCO. In this step, we check the scaling of setpoints and the capability of the aero-servo design of the WTM to replicate the IEA 15 MW at small scale;
- we examine the steady-state rotor performance coefficients, which are at the base of the linearized aerodynamic model of Sect. 3.1, the tool used to down-scale the wind turbine controller. In particular, the wind turbine controller scaling uses the OpenFAST C_P as a proxy for the experimental C_P, thus we check the consistency of the two;
- we analyze the closed-loop response with unsteady inflow created by platform pitch motion. In detail, we first verify the prediction of the stand-alone aerodynamic model of Sect. **??**. Finally, the wind turbine response with platform pitch motion and OpenFAST with prescribed rotor speed oscillations and blade pitch variations; then, we compare the experiment with the OpenFAST model to understand how discrepancies in the modeling of aerodynamics and wind turbine actuation influence the closed-loop control is analyzed; phase-averaged time series of rotor speed , blade pitch , aerodynamic thrust and torque are examined to validate the capability of OpenFAST to predict the turbine behavior; aerodynamic thrust and torque response to apparent wind is computed by means of the linearized model to assess the presence of unsteadiness. response.

5.1 Fixed turbine response

The response of the WTM controlled with the ROSCO is measured at six wind speeds. Figure 5 shows the operating points obtained in the wind tunnel , which are compared, at model scaleto curves computed in OpenFAST for the , to the OpenFAST model of the WTM and to the IEA 15 MWand for the wind turbine scale model. The rotor speed characteristic of the wind turbine scale model measured in the wind tunnel matches with good accuracy the IEA 15 MW The OpenFAST model of the WTM is perfectly overlapping with the referencealigned with the IEA 15 MW, whereas rotor speed in the experiment is slightly higher (the maximum error is 10.5 rpm at 2.9 m/s). The discrepancy in the experiment can be due to a small static offset in the generator speed feedback and/or in the wind speed measurement used for calculation of TSR and the generator speed setpointset point in the TSR-tracking controller. In below-rated wind speeds, collective blade pitch is 2.3° instead of 0° , and this deviation from the reference and this is likely due to misalignment of individual blades and/or an incorrect setting

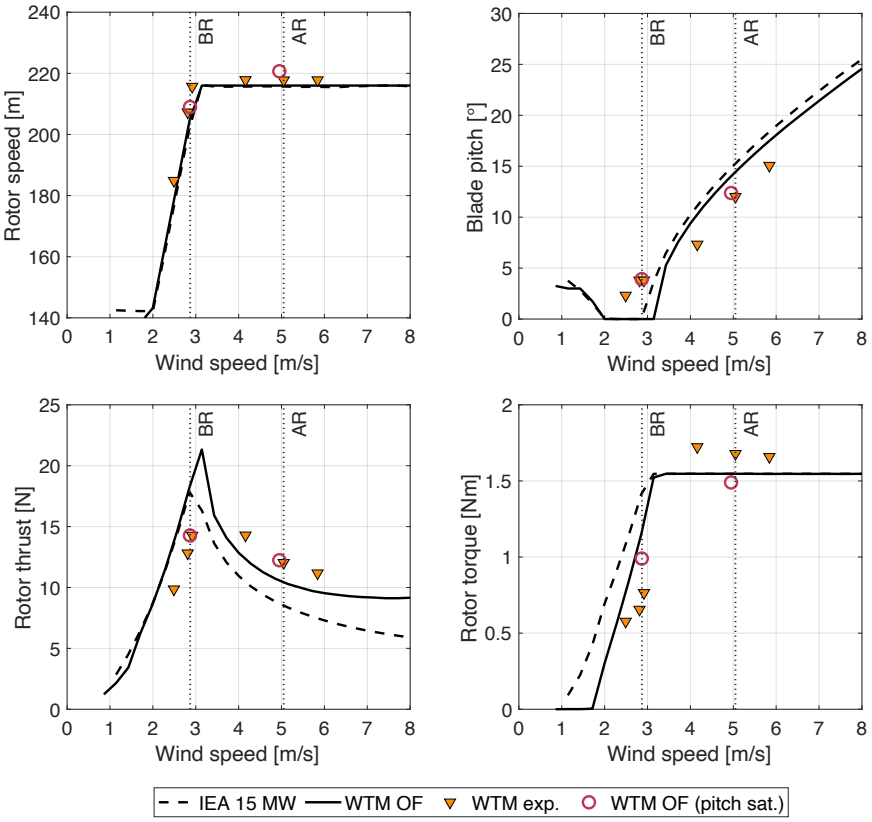

Figure 5. Steady-state operating points for the wind turbine scale model (WTM) obtained in the wind tunnel experiment (exp.) and from the OpenFAST model (OF) are compared to the IEA 15 MW at model scale. Vertical dotted lines identify the below rated (BR) and above rated (AR) operating conditions considered for tests with platform motion. In “WTM OF (pitch sat.)" the minimum pitch in ROSCO is set to the BR pitch of the experiment to simulate the blade pitch offset.

of the zero-pitch position. In ~~above-rated wind~~ above rated wind speeds, the rated rotor speed is achieved with values of blade pitch that have an offset of about -3.5° with respect to the IEA 15 MW.

The scale model rotor is designed to match the thrust force of the IEA 15 MW ~~in below rated wind, when TSR~~when TSR = 9 and $\beta = 0°$~~, and this is true for the OpenFAST model of the WTM where target values of rotor speed and blade pitch are achieved. Correct scaling of rotor torque is not the primary objective of blade design, and the scale model torque predicted by OpenFAST is lower than target for any wind speed: this is due to the lower efficiency of the SD7032 compared to airfoils of the~~ . Below rated, the thrust force in the experiment is lower than the IEA 15 MW due to the blade pitch offset; instead, in OpenFAST, where the blade pitch is 0°, the thrust force is aligned to the one of the IEA 15 MW. ~~In below-rated wind , the WTM in the experiment works with TSR and collective pitch slightly different than those considered for rotor design, which results in a decreased in thrust and torque. In OpenFAST simulations, the turbine scale model achieves the rated rotor speed~~

and rotor torque with pitch angle values slightly Blades misalignment is a well-known problem for model wind turbines: its impact on wind turbine performance and thrust is also investigated by Jüchter et al. (2022), who propose to reduce it with a new blade mounting procedure.

The torque in OpenFAST is lower than the IEA 15 MW ; thrust force is higher than target for all wind speeds. This is due to the aerodynamic characteristics of the airfoil used in the scale model blade. lower efficiency of the SD7032 compared to full-scale airfoils. In the experiment, torque is higher than the rated value for the IEA 15 MW; the cause of this error can be the torque setpoint set point obtained with Eq. 3, which requires knowledge of the transmission efficiencyefficiency, hard to characterize. Rotor thrust has the same trend in the experiment and in the WTM OpenFAST model, but wind tunnel values are higher than in simulations. The difference is attributed to values of blade pitch that are lower than targetthe blade pitch offset that is present in the experiment.

The minimum blade pitch of ROSCO in the WTM OpenFAST model is increased to the collective pitch of the experiment to simulate the blades pitch offset. This model is simulated in the two wind conditions considered in the tests with platform movement and results are closer to those of the experiment. The largest difference is seen for rotor torque in below rated condition, which is 29% higher in OpenFAST compared to the experiment. This difference is attributed to airfoil efficiency which is higher in the OpenFAST model, that is based on polars measured on a 2D airfoil (Fontanella et al. (2021)), than in the experiment. 3D rotor, and it can be due to manufacturing imperfections or unpredicted variations of aerodynamic characteristics that may occur at low Reynolds. The primary function of wind turbine controllers like the ROSCO is to regulate power, thus any difference in airfoil efficiency changes the operating points of the wind turbine making it difficult to reproduce the experiment with a numerical simulation tool for validation tasks. Matching between OpenFAST and the experiment can be improved estimating polars based on experimental data, for example by means of the methodology proposed by Bottasso et al. (2014).

5.2 Performance coefficients and linearized aerodynamic response

Power and thrust coefficients of the wind turbine scale model are measured for various combinations of TSR and blade pitch angle. Wind speed is 4 m/s in all tests and TSR is varied changing rotor speed in open-loop (i.e., without using the ROSCO). The same conditions of the experiment are simulated with the OpenFAST model of the WTM, and results of wind tunnel measurements and simulations are compared in Fig. 5. The shape of The maximum C_P and C_T calculated in OpenFAST is very close to those measured in the wind tunnel. The 0.42 for TSR close to 9 and $\beta = 0°$, whereas the maximum C_P in the experiment is 0.44 for (TSR $\approx$ 9.5, TSR near 9.5 and $\beta = 0°$); the . The transition from maximum C_P to zero is milder in the experiment OpenFAST than in the experiment, where more combinations of (TSR, β) have $C_P \approx 0$; this can be due to the efficiency of the blade that in conditions far from the steady-state characteristic of the turbine is lower in the wind tunnel than in OpenFAST. Numerical and experimental , as already seen in Fig. 5. At TSR = 9, $C_T = 0.8$ in OpenFAST, whereas in the wind tunnel $C_T = 1$. The higher values of C_P and C_T are similar. measured in the wind tunnel are likely due to blockage (Robertson et al. (2023)). Despite the low Reynolds and the presence of blockage, the performance of the wind turbine model at its optimal operating point and the shape of the C_P and C_T curves are very close to the IEA 15 MW, and this makes the model sufficiently representative of the full-scale turbine.

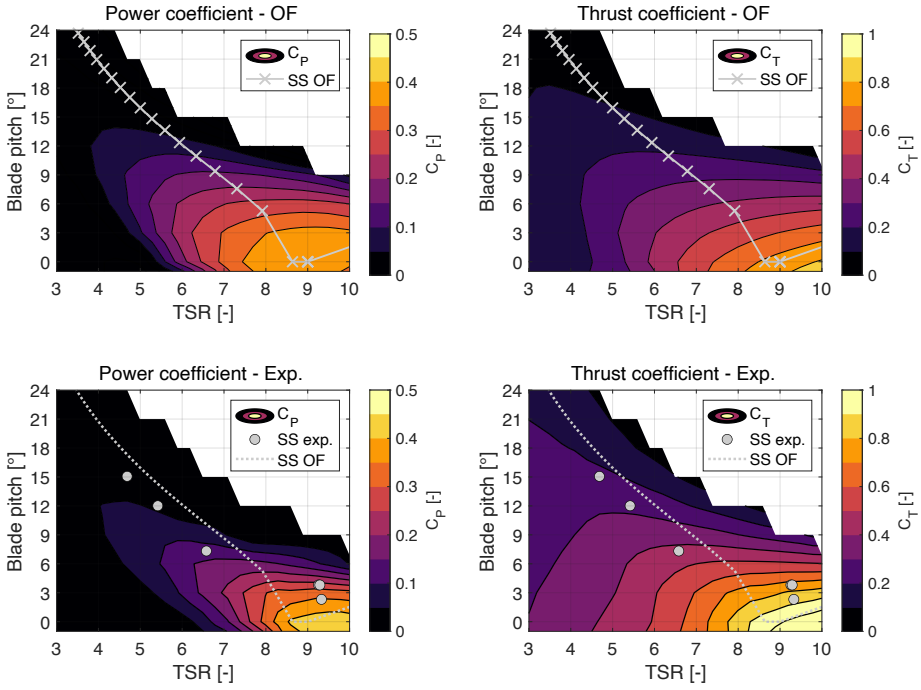

Figure 6. Power coefficient (C_P) and thrust coefficient (C_T) ~~surfaces~~ for the wind turbine scale model measured in the wind tunnel (Exp.) and obtained ~~from~~ in OpenFAST (OF). “SS OF" and “SS exp." are the steady-state control trajectories of Fig. 5. Negative values are not shown.

Aerodynamic sensitivities are calculated ~~based on the expressions reported~~ as in Appendix **??**A, from partial derivatives of the performance coefficients of Fig. 6 and the steady-state operating points of Fig. 5. Partial derivatives of $C_P(\lambda, \beta)$ and $C_T(\lambda, \beta)$ are obtained from the numerical gradient of rotor performance coefficients which is computed with the central difference method. ~~Sensitivities of the IEA 15 MW are compute with the same procedure used for the WTM.~~ The aerodynamic sensitivities of the WTM and of the IEA 15 MW are shown in Fig. 7~~, together with those of the IEA 15 MW.~~ . In above-rated wind speeds, the experiment is in good agreement with the OpenFAST model of the WTM and ~~match~~ matches well the IEA 15 MW, whereas larger differences are seen ~~below rated~~in the below rated region. Discrepancies in ~~partial regime~~ below wind speeds are more pronounced for $K_{\beta Q}$ and $K_{\beta T}$, the sensitivities to blade pitch, and they can be due to the ~~steady-state pitch , which is different from 0°~~ blade pitch offset present in the experiment. $K_{\omega Q}$ is very similar in the experiment and in OpenFAST, and this supports the use of the OpenFAST results in the tuning of the PI TSR-tracking controller; a similar convergence of results is found for $K_{\beta Q}$ in the above-rated ~~wind, thus~~ region, thus aerodynamic data obtained from the OpenFAST model ~~is suitable also for design of~~ are suitable also to design the PI pitch controller.

~~Aerodynamic sensitivities of Fig. 7 constitute the basis of the linearized aerodynamic model of Sect. **??**. In general, the linearized aerodynamic response of the experimental and OpenFAST is expected to be similar where convergence of aerodynamic~~

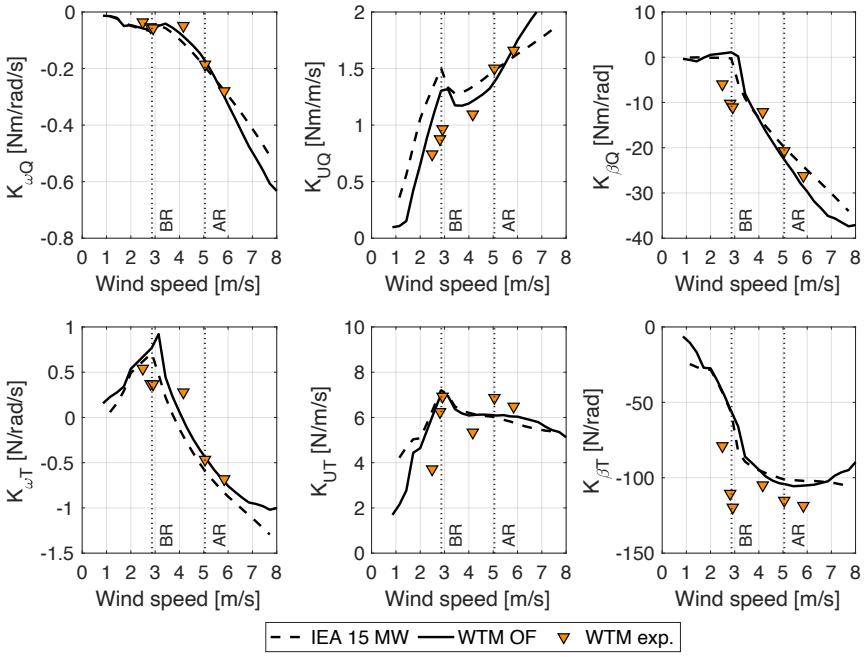

Figure 7. Aerodynamic sensitivities at the steady-sate operating points of Fig. 6 obtained from $C_P(\lambda, \beta)$ and $C_T(\lambda, \beta)$ coefficients with the expressions of Appendix A. Experimental results (WTM exp.) are compared to values computed from the OpenFAST model of the turbine scaled model (WTM OF) and to the IEA 15 MW at model scale. Vertical dotted lines identify the below rated (BR) and above rated (AR) operating conditions considered for tests with platform motion.

~~sensitivities is achieved. Dissimilarity of $K_{\beta Q}$ and $K_{\beta T}$ in below-rated wind do not impact the turbine response, because pitch is not actuated at that wind speeds. The turbine exhibits different sensitivity of torque to wind speed (K_{UQ}) in the below-rated region, and of thrust to blade pitch ($K_{\beta T}$) in above-rated regime.~~

5.3 ~~Response~~ Verification of the aerodynamic model with platform pitch motion

~~The~~ When the wind turbine is subjected to prescribed platform pitch motion ~~of frequency and amplitude reported in Table 2. In the dynamic wind condition created by platform movement the turbine controller~~ the turbine controller dynamically actuates generator torque and collective blade pitch to regulate rotor speed. Platform pitch variations result in oscillations of rotor speed, blade pitch, rotor thrust and torque ~~. The turbine response recorded over a number of periods is phase-averaged using the platform pitch motionfor the synchronizing signal, in order to filter harmonic contributions that are not due to platform motion~~whose amplitude is proportional to the apparent wind speed created by platform motion. We discuss the condition with $A_m = 2.2°$ and $f_m = 1.25$ Hz, which has relatively large ΔU and where it is possible to see the largest differences between experiment and numerical simulations.

Figure 8 shows the WTM response with below-rated wind and three motion conditions. Phase-averaged turbine response (T is aerodynamic rotor thrust, Q is aerodynamic torque) with platform pitch motion of various frequency (f_{m}) in below-rated wind, measured in the experiment (Exp.) and obtained in OpenFAST (OF) simulations (SB = steady BEM, DB = dynamic BEM, SA = static airfoil polars, UA = unsteady airfoil polars). "Exp. fixed" is the steady-state value with fixed turbine. Blade pitch is saturated and the controller responds with actuation of generator torque. The minimum blade pitch in OpenFAST is set to the same value Calculation of aerodynamic loads in the stand-alone AeroDyn module is verified prescribing the platform pitch, rotor speed, and blade pitch oscillations of the experiment to simulate the blade pitch offset. Blade pitch is slightly higher than in the fixed case, and this results in slightly lower mean value for rotor speed, rotor thrust and aerodynamic torque. The other signals exhibit a first-order sine wave, thus the wind turbine response is driven by a single frequency corresponding to platform motion. Rotor speed has oscillations of few rpm, the mean value is lower than the steady-state value of in the numerical model. Time series of rotor speed and blade pitch are filtered to isolate the harmonic at frequency f_{m} and only this harmonic component is analyzed. The aerodynamic response of AeroDyn is compared to the experiment in Fig. 5, but it is similar in OpenFAST and in the experiment; the amplitude of oscillations is the largest with f_{m} = 1.25 Hz, and minimum with f_{m} = 0.15 Hz, thus it appears to be proportional to the apparent wind speed created by platform motion (ΔU in Table 2); the amplitude is larger in the experiment than in OpenFAST, and the phase 8 and Fig. 9, which show the zero-peak amplitude and phase shift with respect to motion is different.

Aerodynamic of the aerodynamic thrust and torque have a maximum with motion phase of 180°, that corresponds to the hub moving upwind with maximum velocity; thus the aerodynamic response of the wind turbine is driven by apparent wind created by motion rater than rotor speed oscillations. Peak thrust is slightly higher in OpenFAST than in the experiment and small higher-order effects are seen with f_{m} = 2 Hz, but the overall agreement is good. Differences are larger for torque. Torque oscillations have lower amplitude in OpenFAST. AeroDyn simulations are repeated with dynamic wake (DW) and static wake (SW) models. In the cases without control, rotor speed and blade pitch are fixed; for the below-rated wind speed, the experimental results with fixed rotor speed/blade pitch are omitted, because when the WTM is controlled with an open-loop rotor speed set point, rotor speed is not fixed but has oscillations of 1.5 rpm, which is comparable to when the ROSCO is used.

Below rated, when rotor speed and blade pitch are fixed, the amplitude and phase shift of aerodynamic loads variations computed with AeroDyn and static or dynamic wake are similar. The result does not change much when rotor speed varies sinusoidally: the thrust phase is slightly lower than in the experiment, regardless of the output variable; in cases with f_{m} = 1.25 Hz and 2.00 Hz the peak is at 180° in OpenFAST, and at 170° in the experiment . Torque in OpenFAST is also computed from tower-top loads with the algorithm utilized for experimental data fixed-rotor speed case, and the torque phase is slightly higher. The estimate of aerodynamic torque of the experiment is affected by uncertainty in the rotor inertia (see Sect. 4.2)and it is similar to the aerodynamic torque computed in AeroDyn; this result is not reported in . Whiskers in Fig. 9 , but confirms the post process of experimental data is correct. show how the torque amplitude and phase changes due to a variation of rotor inertia of ±20% its mean value (0.279 kgm^2), which is considered a reasonable error for this parameter. Overall, in the below rated condition, the aerodynamic loads are captured by AeroDyn. This can be in part due to the fact that rotor speed oscillations

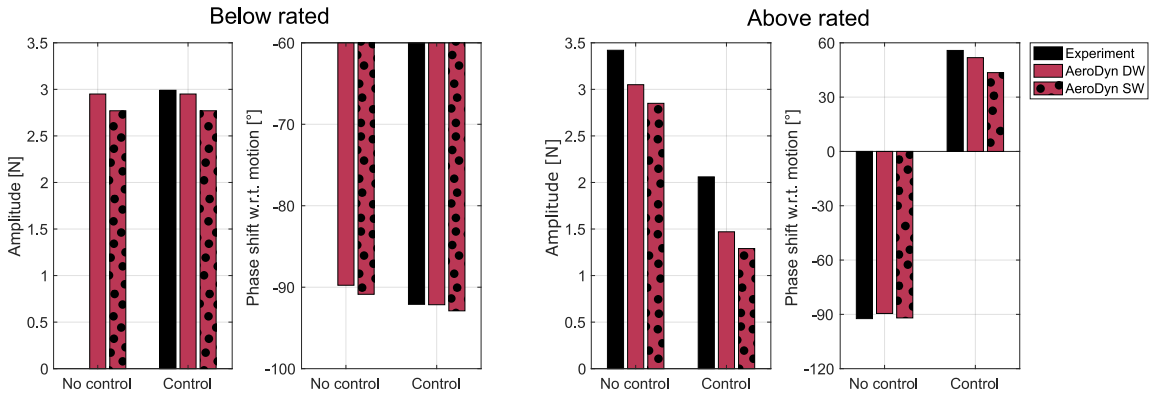

Figure 8. Amplitude and phase shift with respect to platform motion of aerodynamic rotor thrust with $A_m = 2.2°$, $f_m = 2.25$ Hz, with a below rated wind speed of 2.87 m/s and an above rated wind speed of 5.05 m/s, from the experiment and the stand-alone AeroDyn model with dynamic wake (DW) and static wake (SW).

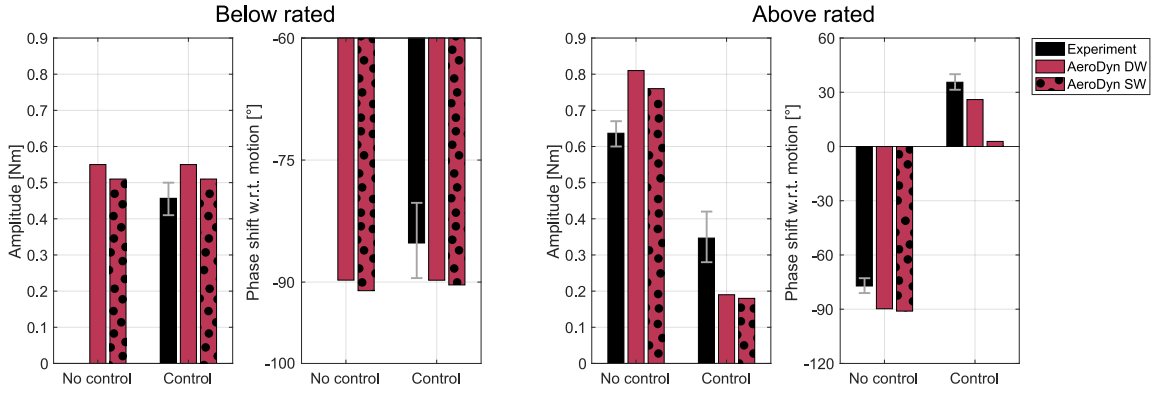

Figure 9. Amplitude and phase shift with respect to platform motion of aerodynamic rotor torque with $A_m = 2.2°$, $f_m = 2.25$ Hz, with a below rated wind speed of 2.87 m/s and an above rated wind speed of 5.05 m/s, from the experiment and the stand-alone AeroDyn model with dynamic wake (DW) and static wake (SW). Whiskers show the experimental aerodynamic torque with a variation of rotor inertia of $\pm 20\%$.

are not large enough to create a challenging unsteady condition (as it is instead done in Bergua et al. (2023)), and indeed the AeroDyn-DW solution is very close to AeroDyn-SW.

~~OpenFAST solutions with unsteady airfoil polars are very close to those with static polars. The amplitude and frequency of motion ensures dynamic stall is confined to blade root and hysteresis in airfoil aerodynamic response is negligible due to low frequency of motion (Sebastian and Lackner (2013)). The amplitude of thrust and torque oscillations in OpenFAST is slightly higher with dynamic BEM than with steady BEM as it has been observed by Bergua et al. (2023), for harmonic rotor speed with amplitude of 15% the mean value . However, the amplitude of experimental aerodynamic torque is not matched by any OpenFAST model.~~

Figure 9 shows the phase-averaged response with above-rated wind and three motion conditions. Phase-averaged turbine response (T is aerodynamic rotor thrust, Q is aerodynamic torque) with platform pitch motion of various frequency (f_{m}) in above-rated wind, measured in the experiment (Exp.) and obtained in OpenFAST (OF) simulations (SB = steady BEM, DB = dynamic BEM, SA = static airfoil polars, UA = unsteady airfoil polars). "Exp. fixed" is the steady-state value with fixed turbine. In this case, generator torque is saturated to its rated value, and the controller responds with actuation of collective blade pitch. The mean value of all signals is aligned with the fixed turbine case, and it is similar in the experiment and OpenFAST. Signals generally exhibit a first-order sine wave, but some higher-order effects are seen in the case with $f_{\mathrm{m}} = 1.25$ Hz, and are more pronounced in OF than in the experiment. The amplitude of rotor speed and torque oscillations is higher than in below-rated wind; the controlled wind turbine is more sensitive to wind speed fluctuations than in below-rated wind, and this is due to the combination of different aerodynamic behavior of the rotor and the action of the pitchcontroller. As in below-rated windAbove rated, with fixed rotor speed and blade pitch, the amplitude of rotor speed oscillations is proportional to ΔU; however, contrarily than in below-rated, it is higher in OpenFAST than in the experiment. Blade pitch variation is proportional to rotor speed oscillations; the amplitude is higher in OpenFAST than in the experimentand phase shift with respect to motion is different.

The thrust response and the torque response show the same phase shift and phase of aerodynamic loads are again similar for the AeroDyn model with static or dynamic wake. AeroDyn under-predicts the amplitude of thrust measured in the experiment, and over-predicts the amplitude of torque; the phase shift of thrust with respect to platform motion , it is different than $180°$, and is in opposition of phase with respect to blade pitch. This suggests the aerodynamic response of the controlled wind turbine is driven by blade pitch more than platform motion. OpenFAST simulations are repeated with ideal pitch actuator (i.e., $G_{\mathrm{act}}(s) = 1$), but results are very similar to those with the pitch actuator model and are omitted. The peak-to-peak amplitude motion is approximately $-90°$ and is captured well. The blade pitch actuation alleviates aerodynamic loads, resulting in smaller amplitudes compared to the case without control. The reduction of thrust and torque oscillations in the experiment is lower than in OpenFAST, but the difference is smaller than for below-rated wind. Models with dynamic polars give similar results of modelswith static polars. The amplitude of all quantities is lower with dynamic BEM than with static BEM and the former is predicted by AeroDyn is greater than in the experiment, it is similar for the DW and SW models, with the DW model slightly closer to the experiment. This is in agreement with the results of Bergua et al. (2023) where simulations are carried out with several codes with prescribed surge motion and prescribed harmonic blade pitch of $1.5°$ amplitude. Fast changes of blade pitch angle are The phase shift is captured well by AeroDyn-DW whereas it is under predicted by AeroDyn-SW. In the above rated condition, differences between numerical simulations and the experiment are larger than below rated. This can be in part due to blade pitch actuation, which is known to cause dynamic inflow effects and large dynamic loads (Snel and Schepers (1995)). However, , and, in the case of harmonic platform motion with active blade pitch control, the OpenFAST solution with dynamic inflow model results in smaller peak-to-peak variations that the one with steady inflow; this results is similar to what is found by Berger et al. (2022) that has analyzed the dynamic inflow effect due to coherent sinusoidal wind field. Interestingly, aerodynamic loads in the experiment are even lower than in the dynamic BEM models. torque, can also be due to uncertainties in the estimation of aerodynamic loads from experimental measurements.

The aerodynamic thrust and torque response to apparent wind is computed from results of the experiment and OpenFAST simulations (dynamic BEM and unsteady airfoil polars) with the linearized model of Sect. **??** and is shown in Fig. 10. To compare the below-rated and above-rated conditions,

5.4 Coupled response with platform pitch motion

The turbine response measured in the experiment is compared to the OpenFAST model of the amplitude of rotor loads (ΔF_x and ΔM_x) is normalized according to the amplitude of hub motion A_{hub}. Linear regression based on experimental and numerical data is also computed. WTM, which includes the ROSCO. The comparison is done based on the time series of rotor speed, blade pitch, aerodynamic thrust and torque recorded over a number of periods, that are phase-averaged to filter harmonic contributions not due to platform motion.

Figure 10 shows the WTM response with a below-rated wind speed of 2.87 m/s.

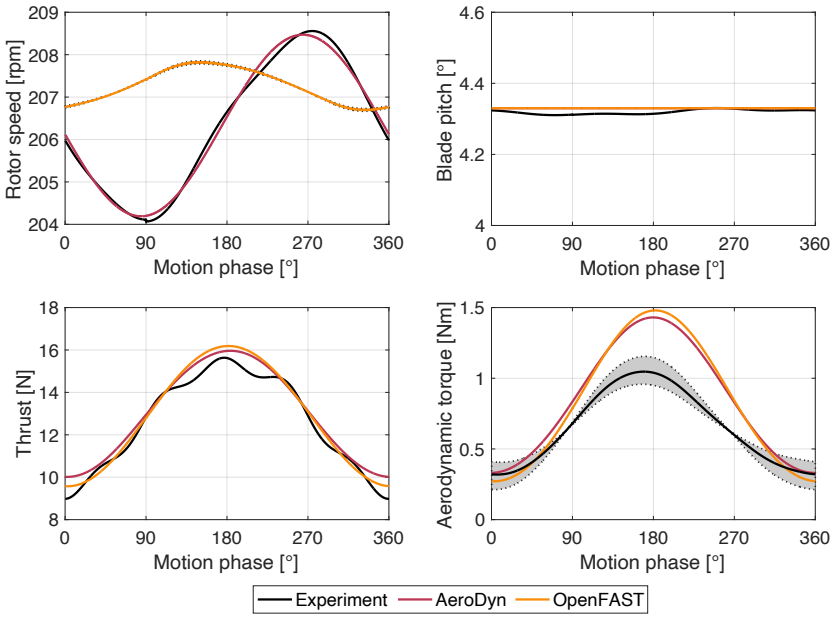

Figure 10. Normalized aerodynamic rotor thrust ($\Delta T/A_{\mathrm{hub}}$) and torque ($\Delta Q/A_{\mathrm{hub}}$) variation and phase shift Phase-averaged turbine response with respect to platform pitch motion during unsteady wind in of $A_{\mathrm{m}} = 2.2°$, $f_{\mathrm{m}} = 2.25$ Hz and a below rated (BR) and above rated (AR) conditionswind of 2.87 m/s, for measured in the experiment and computed in AeroDyn (exp.with dynamic wake) with prescribed rotor speed-blade pitch, and in OpenFAST (OF)with the Simulink controller. The grey area shows the aerodynamic torque estimate with a variation of rotor inertia of $\pm 20\%$.

Aerodynamic rotor loads for below-rated wind are linearly proportional to reduced frequency of motion, and so to the rotor apparent wind. The linear regression gives zero variation of the aerodynamic loads at $f_{\mathrm{r}} = 0$ (i. e., with no platform motion). This also confirms that loads components due to rotor speed variation, that have been subtracted from total aerodynamic

forces based on Eq. ??-?? are linearly proportional to rotor speed (collective pitch is constant in below-rated wind) and are correctly captured by the linearized aerodynamic model. The agreement between OpenFASTand Blade pitch is saturated and the experiment is in general good; the amplitude of ΔT is very close in OF and the experiment, the controller responds with actuation of generator torque. All signals exhibit a first-order sine wave, thus the wind turbine response is driven by a single frequency corresponding to platform motion. In the OpenFAST-Simulink model, the rotor speed has a peak when the motion phase is $150°$, and a peak-to-peak amplitude of ΔQ in OF is slightly 1 rpm. The peak-to-peak amplitude of rotor speed oscillations in the experiment is 4.5 rpm and the maximum is reached when the motion phase is $275°$. The thrust force response is similar in the experiment, in OpenFAST, and in the stand-alone AeroDyn simulation. In all cases, the thrust peak is close to $180°$, when the hub moves upwind with maximum velocity. Also the torque peak is close to $180°$, and the amplitude of oscillations in the experiment is slightly lower than in the OpenFAST model and in AeroDyn (the grey shaded area in the figure shows how the aerodynamic torque estimate changes with a variation of rotor inertia of $\pm 20\%$), but the mean value of torque in the simulations (0.86 Nm) is higher than in the experiment . This difference may be related to the difference in the K_{UQ} sensitivity already (0.66 Nm), as seen in Fig. 7. The phase shift is close to $-90°$; there is some dispersion for experimental torque data at higher frequencies; the phase shift predicted by OpenFAST is $-96°$. 5. The variations of thrust and torque of the OpenFAST-Simulink model are close to the experiment and similar to the stand-alone AeroDyn model, despite the different amplitude and phase of rotor speed oscillations. Being aerodynamic torque variations similar in AeroDyn and OpenFAST-Simulink, one plausible reason for the different rotor speed response is the generator dynamics which is not modeled in OpenFAST (in Simulink the torque set point is followed perfectly by the generator, whereas in the physical WTM the generator has a torque control loop with a dynamic response; this dynamic response is hard to model because the torque controller is embedded in the generator drive and its parameters are not disclosed to users).

In above rated wind, the turbine is controlled with Figure 11 shows the phase-averaged WTM response with an above-rated wind speed of 5.05 m/s. In this case, generator torque is saturated to its rated value, and the controller responds with actuation of collective blade pitch. Variations of rotor loads due to rotor speed and blade pitch are subtracted from aerodynamic forces to isolate the contribution due to apparent wind. The amplitude of loads obtained Signals generally exhibit a first-order sine wave, but higher-order effects are seen in the blade pitch and aerodynamic loads of the OpenFAST-Simulink simulation. The peak-to-peak amplitude of rotor speed and blade pitch variations is lower in the experiment and (3 rpm and $4.1°$) than in the OpenFAST-Simulnik model (6.7 rpm and $6°$); the phase shift between the rotor speed peak and the blade pitch peak is lower in the experiment than in the simulation. When OpenFAST simulations are repeated excluding the pitch actuator model (i.e., $G_{\mathrm{act}}(s) = 1$), the amplitude of rotor speed and blade pitch variations is slightly lower than with the actuator model, but still higher than in OpenFAST is aligned to the linear fit, aerodynamic forces are linearly proportional to rotor speed oscillations and blade pitch variations. The amplitude of thrust oscillations due to apparent wind in the linearized model is lower in OpenFAST than in the experiment; thrust oscillations in Fig.9 have similar amplitude in OpenFAST and the experiment, thus the discrepancy seen in Fig. 10 may be due to differences in . Oscillations of thrust and torque in the experiment have lower amplitude than in OpenFAST-Simulink. The blade pitch excursions in this operating condition are large enough to influence the aerodynamic response of the aerodynamic sensitivities. The amplitude of thrust oscillations due to apparent wind

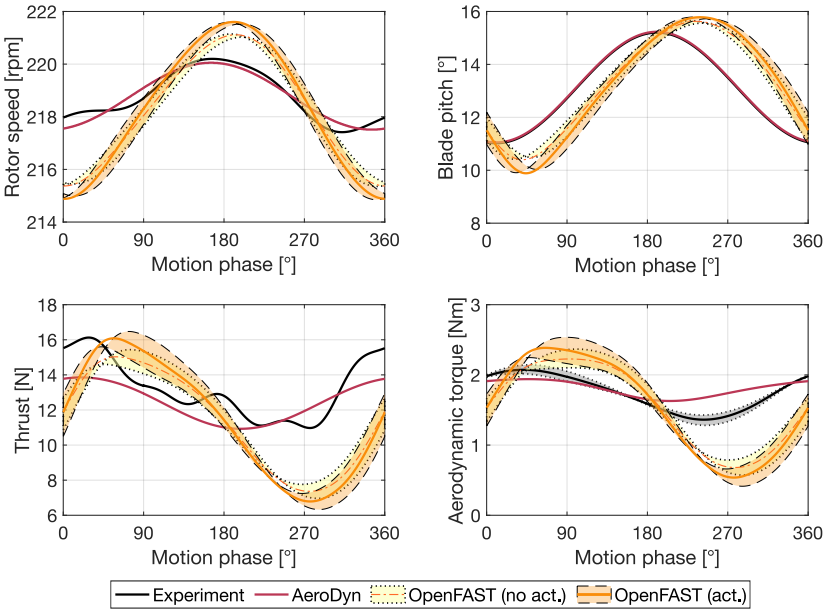

Figure 11. Phase-averaged turbine response with platform pitch motion of $A_m = 2.2°$, $f_m = 2.25$ Hz and an above rated wind of 5.05 m/s, measured in the experiment and computed in AeroDyn (with dynamic wake) with prescribed rotor speed-blade pitch, and in OpenFAST with the Simulink controller. Two OpenFAST-Simulink models are shown, one with and one without the pitch actuator model. The shaded areas show the variation of metrics due to a change in rotor inertia of $\pm 20\%$.

~~is instead the same for experimental and OpenFAST results, meaning~~ wind turbine, and modeling the blade pitch ~~and rotor speed contributions to torque variations are estimated with the same accuracy. The phase shift of thrust and torque is between $-110°$ and $-95°$, it rises linearly with frequency up to $f_r = 0.75$ and is constant above.The trend of phase shift is similar for OpenFAST and experimental data, and the agreement is better for torque than for thrust. Since the agreement for the phase shift of loads due to apparent wind is good, the difference in phase shift seen in Fig. 10 is attributed to blade pitch actuation.~~ control system is critical to capture the wind turbine aerodynamic loading. The pitch actuator may behave differently with wind (i.e., when there is an aerodynamic moment on the blade) than in still air; this difference would not be captured by pitch actuator model and explains the discrepancies in the rotor speed-blade pitch response of OpenFAST compared to the experiment.

6 Conclusions

~~This articlepresented a wind tunnel experiment whose aim is to investigate the aerodynamic response of a floating wind turbine subjected to platform pitch motion and with active control functionalities. A~~ In this article, a theoretical framework is proposed to downscale the reference open-source controller ~~ROSCO~~ (ROSCO) and use it to control a ~~scaled version~~ 1:100 scale model of the IEA 15 MW turbine. The controller preserves the algorithms of its full-scale version, but it is run in real-time at model

scale to respect the time ~~scale~~ scaling of the experiment. Due to this choice, the controller parameters ~~were downscaled; the~~ are downscaled. The controller scaling procedure is model based, and uses information about the aerodynamic response and inertial properties of the ~~scale model to reproduce~~ model turbine to preserve, at small-scale, the rotor response of the full-scale turbine.

~~Testing is conducted with fixed foundation and with~~ The aero-servo-dynamic response of the wind turbine scale model with ROSCO is studied in a wind tunnel experiment with load cases where tower base is fixed and with large prescribed platform pitch motion ~~measuring the rotor response.~~ that mimics a floating foundation.

The experiment is modeled in OpenFAST and results of simulations are compared to those of testing ~~. The~~ to verify the controller scaling and identify the main sources of uncertainty in the modeling of the wind turbine scale model closed-loop response. The steady-state rotor speed-blade pitch-thrust-torque characteristics of the scaled turbine match those of the IEA 15 MW and are correctly captured by the OpenFAST model~~and are representative of the IEA 15 MW~~. The largest differences are ~~seen for torque and are~~ attributed to an offset in blades pitch ~~that occurred~~ present in the experiment, to a lower airfoil efficiency for the physical blade compared to its OpenFAST model, and to uncertainty of the drivetrain efficiency ~~.~~ required for generator control. The wind turbine controller is scaled making use of a linearized aerodynamic model built based on OpenFAST data. The linearized aerodynamics of the turbine scale model is captured by OpenFAST and is close to the IEA 15 MW.

With platform pitch motion, the turbine response is ~~different in below-rated and above-rated wind, depending on the turbine control strategy~~modeled with different accuracy in the below rated and above rated regions. Below rated, ~~blade pitch is saturated, TSR is regulated acting on generator torque with small oscillations of rotor speed (the maximum peak-to-peak amplitude is 2% of mean value) due to the apparent~~ the aerodynamic response is driven by the rotor-apparent wind created by ~~platform motion~~ motion more than rotor speed oscillations, which are relatively small. The aerodynamic ~~response is linearly proportional to rotor-apparent wind and follows the quasi-static theory. Amplitude of thrust oscillations is correctly predicted in OpenFAST , whereas torque oscillations~~ model of OpenFAST captures the loads measured in the experiment, and the agreement is better for thrust than for torque, whose estimate is affected by the uncertain knowledge of rotor inertia. The rotor-speed response in OpenFAST is different than in the experiment~~are of lower amplitude than in simulations.~~ , and this is attributed to the lack of a model for the generator actuator. However, with the control strategy and operating condition we considered here, rotor speed oscillations do not cause significant unsteadiness, thus differences in the rotor speed dynamics are not critical for modeling the aerodynamic loads response due to platform motion. Above rated, ~~generator~~ rotor speed is regulated with collective blade pitch. The amplitude of aerodynamic ~~response is due to the linear combination of variations of~~ loads variations is driven by the combination of apparent wind, ~~rotor speed,~~ and blade pitch ~~. However, the phase does not follow the quasi-steady theory. The amplitude of blade pitch and aerodynamic loads is different~~ oscillations. Differences between the aerodynamic loads computed in OpenFAST and those measured in the experiment ~~.~~ are larger than in the below rated condition. In particular, the decrease in loads due to blade pitch variations is overestimated in AeroDyn compared to the experiment. Slightly better agreement is obtained with the use of dynamic BEM compared to a static wake model. Phase of blade pitch variations in OpenFAST is different than in the experiment~~. This can be either~~ , and this influences the amplitude and phase of aerodynamic loads in the simulation. The different response obtained in OpenFAST can be due to the scale

model blade-pitch actuators behaving differently ~~than expected, or modeling of the coupled aero-servo-dynamic response in OpenFAST~~with wind than in still air (i.e., where the pitch actuator model is obtained), the aerodynamic model of OpenFAST not completely capturing the experiment, or a combination of the two.

In conclusion, this work has provided guidance on how to include ~~reference~~ wind turbine control functionalities in scale model testing of floating wind turbines. It has also confirmed the aerodynamic load response with platform motion and active control is more difficult to model than when rotor speed and blade pitch are fixed~~. Above rated wind, where the turbine is controlled with collective blade pitch , the turbine response is not quasi-steady and is more difficult to predict.~~ , in particular in the above rated region where large blade pitch excursion occur. It is shown that knowledge of the blade pitch actuator response is important to model the aero-servo-dynamic response of a floating turbine in above rated wind speeds.

In ~~tuture~~ future work, more codes, possibly of higher fidelity than the BEM we considered here, can be used to ~~model~~ study the wind tunnel experiment and this will help understand which physics of the wind turbine system are important to consider when modeling the aerodynamic response of a floating wind turbine with active control. The present research examined the case of active turbine control and prescribed motion~~in one DOF. In future , the turbine aerodynamic response should be examined in case of realistic platform motion due to wind-wave excitation and active turbine control~~, of low-frequency and large amplitude, in the pitch direction. Floating wind turbines can experience large wave-frequency motions that should be examined in future experiments. Moreover, only thrust and torque loads have been investigated in the present study, but the other four components of the aerodynamic loading are important for the response of some floater concepts (Bachynski et al. (2015)) and should be addressed in future wind tunnel studies.

Data availability. The OpenFAST model, the MATLAB Simulink version of the reference open-source controller ROSCO, and experimental data can be downloaded at Fontanella et al. (2023b).

Appendix A: ~~Appendix A~~Analytical expressions of rotor aerodynamic sensitivities

We provide here the analytical expressions of rotor aerodynamic sensitivities. The rotor speed to rotor torque sensitivity is:

$$K_{\omega Q} = \frac{Q_0}{\omega_{\mathrm{r},0}} \frac{\partial C_Q}{\partial \lambda}\bigg|_0 \frac{\lambda_0}{C_{Q,0}}, \tag{A1}$$

the wind speed to rotor torque sensitivity is:

$$K_{UQ} = \frac{Q_0}{U_0}\left(2 - \frac{\partial C_Q}{\partial \lambda}\bigg|_0 \frac{\lambda_0}{C_{Q,0}}\right), \tag{A2}$$

and the collective blade pitch angle to rotor torque sensitivity is:

$$K_{\beta Q} = \frac{1}{2}\rho\pi R^3 U_0^2 \frac{\partial C_Q}{\partial \beta}\bigg|_0, \tag{A3}$$

where $\partial C_Q/\partial\lambda$ and $\partial C_Q/\partial\beta$ are the two components of the C_Q gradient. The torque coefficient is computed from the power coefficient as $C_Q = C_P/\lambda$.

The rotor speed to rotor thrust sensitivity is:

$$K_{\omega T} = \frac{T_0}{\omega_0} \frac{\partial C_T}{\partial \lambda}\bigg|_0 \frac{\lambda_0}{C_{T,0}}, \tag{A4}$$

the wind speed to rotor thrust sensitivity is:

$$K_{UT} = \frac{T_0}{U_0}\left(2 - \frac{\partial C_T}{\partial \lambda}\bigg|_0 \frac{\lambda_0}{C_{T,0}}\right), \tag{A5}$$

and the collective blade pitch angle to rotor thrust sensitivity is:

$$K_{\beta T} = \frac{1}{2}\rho\pi R^2 U_0^2 \frac{\partial C_T}{\partial \beta}\bigg|_0, \tag{A6}$$

where $\partial C_T/\partial\lambda$ and $\partial C_T/\partial\beta$ are the two components of the C_T gradient.

Appendix B: ~~Appendix B~~Frequency response of the turbine controller with input/output scaling

We demonstrate that running the turbine controller at full-scale with scaling of input and output signals does not preserve the turbine frequency response.

Let us consider here the response of the wind turbine to a change in wind speed when it function in full load and rotor speed is controlled with a PI collective blade pitch controller. Assuming the wind speed rate of change is low, the variation of rotor speed is:

$$F9\overline{\omega}_{\mathrm{r}} = -\frac{K_{UQ}}{K_{\omega Q}}\,\overline{U}. \tag{B1}$$

This variation of rotor speed is counteracted by the PI collective pitch controller, which frequency response function for the IEA 15 MW is shown in Fig. ~~11~~B1.

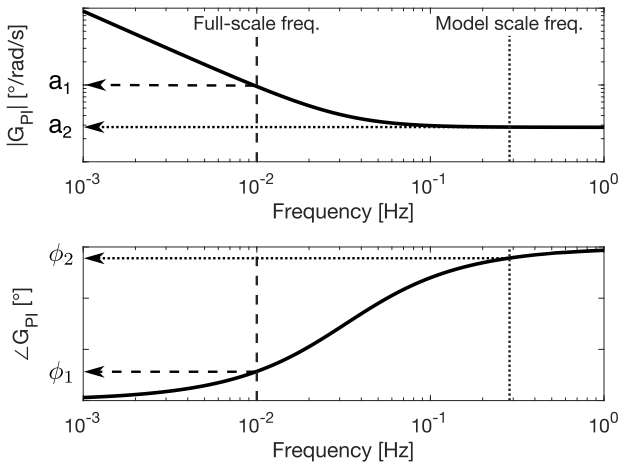

Figure B1. Frequency response function (amplitude and phase) of the IEA 15 MW PI collective blade pitch controller. The frequency response function evaluated at "Full-scale freq." has amplitude a_1 and phase ϕ_1. If it is evaluated at "Model scale freq." it has amplitude a_2 and phase ϕ_2.

We assume the variation of wind speed for the full-scale turbine is harmonic. In general, this can be due to a wind gust or due to the apparent wind created by motion in case of a floating wind turbine. The wind speed variation is:

$$\overline{U} = u \sin(2\pi f_{\mathrm{w}} t), \tag{B2}$$

where f_{w} is the frequency of the wind speed oscillations. Using Eq. B1, the rotor speed response due to the wind speed is:

$$\overline{\omega}_{\mathrm{r}} = -\frac{K_{UQ}}{K_{\omega Q}} (u \sin(2\pi f_{\mathrm{w}} t)). \tag{B3}$$

The blade pitch controller reaction to this oscillation is:

$$\overline{\beta} = a_1 \left(-\frac{K_{UQ}}{K_{\omega Q}} \right) (u \sin(2\pi f_{\mathrm{w}} t + \phi_1)), \tag{B4}$$

where a_1 and ϕ_1 are the amplitude and frequency of the PI pitch controller frequency response function at f_{w}.

Let us consider a scaled version of the full-scale turbine. The wind speed oscillation for the model has scaled amplitude and scaled frequency (e.g., when the turbine is mounted on a scale model of the floating platform):

$$\overline{U} = (u\lambda_v) \sin(2\pi f_{\mathrm{w}} \lambda_f t), \tag{B5}$$

where $\lambda_f = \lambda_v \lambda_L^{-1}$. Assuming the rotor response of the turbine model is ideally scaled:

$$\overline{\omega}_{\mathrm{r}} = \left(-\frac{K_{UQ}}{K_{\omega Q}} \frac{1}{\lambda_L} \right) (u\lambda_v) \sin(2\pi f_{\mathrm{w}} \lambda_f t) \tag{B6}$$

When the turbine controller is operated in real-time in full-scale mode, inputs from the turbine model are scaled up to full-scale values before going into the controller. For rotor speed:

$$\overline{\omega}_{\mathrm{r,fs}} = \left(\left(-\frac{K_{UQ}}{K_{\omega Q}} \frac{1}{\lambda_L} \right) (u\lambda_v) \frac{1}{\lambda_f} \right) \sin(2\pi f_{\mathrm{w}} \lambda_f t), \tag{B7}$$

where $\lambda_v \lambda_L^{-1} \lambda_f^{-1} = 1$. The blade pitch controller response is:

$$\overline{\beta} = a_2 \left(-\frac{K_{UQ}}{K_{\omega Q}} \right) (u \sin(2\pi f_{\mathrm{w}} \lambda_f t + \phi_2)), \tag{B8}$$

where a_2 and ϕ_2 are the amplitude and frequency of the PI pitch controller frequency response function at $f_{\mathrm{w}}\lambda_f$. $\overline{\beta}$ is non dimensional and, with the full-scale controller approach, it is applied to the turbine scale model without any further operation.

Comparing Eq. B4 to Eq. B8 we see they have different amplitude and phase, that are due to the frequency response function of the PI blade pitch controller rather than dimensional scaling.

Appendix C: List of symbols

Table C1 is a list of the symbols that occur most often in the text.

Table C1. List of symbols.

Symbol	Meaning
A_{w}	Amplitude of sinusoidal pitch motion
f_{w}	Frequency of sinusoidal pitch motion
h	Drivetrain closed-loop damping ratio
J^*	Drivetrain (rotor and generator) inertia
$K_{\beta Q}$	Blade pitch-to-torque sensitivity
$K_{\omega Q}$	Rotor speed-to-torque sensitivity
Q_{a}	Aerodynamic rotor torque
Q_{g}	Generator torque
U	Free-stream wind speed
β	Collective blade pitch
η_{g}	Drivetrain efficiency
λ	Tip-speed ratio
λ_L	Length scale factor
λ_v	Velocity scale factor
τ_{g}	Drivetrain transmission ratio
ω_{g}	Generator speed
ω_{r}	Rotor speed
Ω	Drivetrain closed-loop frequency

Author contributions. AF and ED devised the methodology to downscale the wind turbine controller and created the simulation model. FN, AF and MB designed the wind tunnel experiment, that was run by AF, ED and FN. ED and AF analyzed the experimental data and run the numerical simulations. MB supervised the research project. All coauthors thoroughly reviewed the article.

Competing interests. The authors declare that they have no conflict of interest.

Acknowledgements. The project has received funding from the European Union's Horizon 2020 research and innovation program under grant agreement No. 860737 (STEP4WIND project, STEP4WIND).

References

Abbas, N. J., Daniel, Z. S., Mudafort, R. M., Hylander, G., Mulders, S., davidheff, and Bortolotti, P.: NREL/ROSCO: RAAW v1.3, https://doi.org/10.5281/zenodo.7154733, https://doi.org/10.5281/zenodo.7154733, 2022a.

Abbas, N. J., Zalkind, D. S., Pao, L., and Wright, A.: A reference open-source controller for fixed and floating offshore wind turbines, Wind Energy Science, 7, 53–73, https://doi.org/10.5194/wes-7-53-2022, https://wes.copernicus.org/articles/7/53/2022/, 2022b.

Bachynski, E. E., Chabaud, V., and Sauder, T.: Real-time Hybrid Model Testing of Floating Wind Turbines: Sensitivity to Limited Actuation, Energy Procedia, 80, 2–12, https://doi.org/https://doi.org/10.1016/j.egypro.2015.11.400, https://www.sciencedirect.com/science/article/pii/S1876610215021323, 12th Deep Sea Offshore Wind R&D Conference, EERA DeepWind 2015, 2015.

Berger, F., Neuhaus, L., Onnen, D., Hölling, M., Schepers, G., and Kühn, M.: Experimental analysis of the dynamic inflow effect due to coherent gusts, Wind Energy Science, 7, 1827–1846, https://doi.org/10.5194/wes-7-1827-2022, https://wes.copernicus.org/articles/7/1827/2022/, 2022.

Bergua, R., Robertson, A., Jonkman, J., Branlard, E., Fontanella, A., Belloli, M., Schito, P., Zasso, A., Persico, G., Sanvito, A., Amet, E., Brun, C., Campaña Alonso, G., Martín-San-Román, R., Cai, R., Cai, J., Qian, Q., Maoshi, W., Beardsell, A., Pirrung, G., Ramos-García, N., Shi, W., Fu, J., Corniglion, R., Lovera, A., Galván, J., Nygaard, T. A., dos Santos, C. R., Gilbert, P., Joulin, P.-A., Blondel, F., Frickel, E., Chen, P., Hu, Z., Boisard, R., Yilmazlar, K., Croce, A., Harnois, V., Zhang, L., Li, Y., Aristondo, A., Mendikoa Alonso, I., Mancini, S., Boorsma, K., Savenije, F., Marten, D., Soto-Valle, R., Schulz, C. W., Netzband, S., Bianchini, A., Papi, F., Cioni, S., Trubat, P., Alarcon, D., Molins, C., Cormier, M., Brüker, K., Lutz, T., Xiao, Q., Deng, Z., Haudin, F., and Goveas, A.: OC6 project Phase III: validation of the aerodynamic loading on a wind turbine rotor undergoing large motion caused by a floating support structure, Wind Energy Science, 8, 465–485, https://doi.org/10.5194/wes-8-465-2023, https://wes.copernicus.org/articles/8/465/2023/, 2023.

Bottasso, C. L., Cacciola, S., and Iriarte, X.: Calibration of wind turbine lifting line models from rotor loads, Journal of Wind Engineering and Industrial Aerodynamics, 124, 29–45, https://doi.org/https://doi.org/10.1016/j.jweia.2013.11.003, https://www.sciencedirect.com/science/article/pii/S0167610513002493, 2014.

Cioni, S., Papi, F., Pagamonci, L., Bianchini, A., Ramos-García, N., Pirrung, G., Corniglion, R., Lovera, A., Galván, J., Boisard, R., Fontanella, A., Schito, P., Zasso, A., Belloli, M., Sanvito, A., Persico, G., Zhang, L., Li, Y., Zhou, Y., Mancini, S., Boorsma, K., Amaral, R., Viré, A., Schulz, C. W., Netzband, S., Soto Valle, R., Marten, D., Martín-San-Román, R., Trubat, P., Molins, C., Bergua, R., Branlard, E., Jonkman, J., and Robertson, A.: On the characteristics of the wake of a wind turbine undergoing large motions caused by a floating structure: an insight based on experiments and multi-fidelity simulations from the OC6 Phase III Project, Wind Energy Science Discussions, 2023, 1–37, https://doi.org/10.5194/wes-2023-21, https://wes.copernicus.org/preprints/wes-2023-21/, 2023.

Fontanella, A., Liu, Y., Azcona, J., Pires, O., Bayati, I., Gueydon, S., de Ridder, E. J., van Wingerden, J. W., and Belloli, M.: A hardware-in-the-loop wave-basin scale-model experiment for the validation of control strategies for floating offshore wind turbines, Journal of Physics: Conference Series, 1618, 032 038, https://doi.org/10.1088/1742-6596/1618/3/032038, https://dx.doi.org/10.1088/1742-6596/1618/3/032038, 2020.

Fontanella, A., Bayati, I., Mikkelsen, R., Belloli, M., and Zasso, A.: UNAFLOW: a holistic wind tunnel experiment about the aerodynamic response of floating wind turbines under imposed surge motion, Wind Energy Science, 6, 1169–1190, https://doi.org/10.5194/wes-6-1169-2021, https://wes.copernicus.org/articles/6/1169/2021/, 2021.

Fontanella, A., Da Pra, G., and Belloli, M.: Integrated Design and Experimental Validation of a Fixed-Pitch Rotor for Wind Tunnel Testing, Energies, 16, https://doi.org/10.3390/en16052205, https://www.mdpi.com/1996-1073/16/5/2205, 2023a.

Fontanella, A., Daka, E., Novais, F., and Belloli, M.: Aerodynamics of a Floating Wind Turbine Scale Model with Active Control, https://doi.org/10.5281/zenodo.7741358, https://doi.org/10.5281/zenodo.7741358, 2023b.

Gaertner, E., Rinker, J. and. Sethuraman, L., Zahle, F., Anderson, B., Barter, G., Abbas, N., Meng, F., Bortolotti, P., Skrzypinski, W., Scott, G., Feil, R., Bredmose, H., Dykes, K., Shields, M., Allen, C., and Viselli, A.: Definition of the IEA 15-Megawatt Offshore Reference Wind Turbine, Tech. rep., National Renewable Energy Laboratory, https://www.nrel.gov/docs/fy20osti/75698.pdf, Available at https://www.nrel.gov/docs/fy20osti/75698.pdf, 2020.

Goupee, A. J., Kimball, R. W., and Dagher, H. J.: Experimental observations of active blade pitch and generator control influence on floating wind turbine response, Renewable Energy, 104, 9–19, https://doi.org/https://doi.org/10.1016/j.renene.2016.11.062, https://www.sciencedirect.com/science/article/pii/S0960148116310461, 2017.

Gueydon, S., Lindeboom, R., van Kampen, W., and de Ridder, E.-J.: Comparison of Two Wind Turbine Loading Emulation Techniques Based on Tests of a TLP-FOWT in Combined Wind, Waves and Current, ASME 2018 1st International Offshore Wind Technical Conference, https://doi.org/10.1115/IOWTC2018-1068, https://doi.org/10.1115/IOWTC2018-1068, v001T01A012, 2018.

Gueydon, S., Bayati, I., and de Ridder, E.: Discussion of solutions for basin model tests of FOWTs in combined waves and wind, Ocean Engineering, 209, 107 288, https://doi.org/https://doi.org/10.1016/j.oceaneng.2020.107288, https://www.sciencedirect.com/science/article/pii/S0029801820303322, 2020.

Jüchter, J., Peinke, J., Lukassen, L. J., and Hölling, M.: Reduction and analysis of rotor blade misalignments on a model wind turbine, Journal of Physics: Conference Series, 2265, 022 071, https://doi.org/10.1088/1742-6596/2265/2/022071, https://dx.doi.org/10.1088/1742-6596/2265/2/022071, 2022.

Kim, T., Madsen, F., Bredmose, H., and Pegalajar-Jurado, A.: Numerical analysis and comparison study of the 1:60 scaled DTU 10 MW TLP floating wind turbine, Renewable Energy, 202, 210–221, https://doi.org/https://doi.org/10.1016/j.renene.2022.11.077, https://www.sciencedirect.com/science/article/pii/S0960148122017165, 2023.

Larsen, T. J. and Hanson, T. D.: A method to avoid negative damped low frequent tower vibrations for a floating, pitch controlled wind turbine, Journal of Physics: Conference Series, 75, 012 073, https://doi.org/10.1088/1742-6596/75/1/012073, https://dx.doi.org/10.1088/1742-6596/75/1/012073, 2007.

Madsen, F., Nielsen, T., Kim, T., Bredmose, H., Pegalajar-Jurado, A., Mikkelsen, R., Lomholt, A., Borg, M., Mirzaei, M., and Shin, P.: Experimental analysis of the scaled DTU10MW TLP floating wind turbine with different control strategies, Renewable Energy, 155, 330–346, https://doi.org/https://doi.org/10.1016/j.renene.2020.03.145, https://www.sciencedirect.com/science/article/pii/S096014812030478X, 2020.

Mendoza, N., Robertson, A., Wright, A., Jonkman, J., Wang, L., Bergua, R., Ngo, T., Das, T., Odeh, M., Mohsin, K., Flavia, F. F., Child, B., Bangga, G., Fowler, M., Goupee, A., Kimball, R., Lenfest, E., and Viselli, A.: Verification and Validation of Model-Scale Turbine Performance and Control Strategies for the IEA Wind 15 MW Reference Wind Turbine, Energies, 15, https://doi.org/10.3390/en15207649, https://www.mdpi.com/1996-1073/15/20/7649, 2022.

Meng, F., Lio, W. H., and Barlas, T.: DTUWEC: an open-source DTU Wind Energy Controller with advanced industrial features, Journal of Physics: Conference Series, 1618, 022 009, https://doi.org/10.1088/1742-6596/1618/2/022009, https://dx.doi.org/10.1088/1742-6596/1618/2/022009, 2020.

Pires, O., Azcona, J., Vittori, F., Bayati, I., Gueydon, S., Fontanella, A., Liu, Y., de Ridder, E., Belloli, M., and van Wingerden, J.: Inclusion of rotor moments in scaled wave tank test of a floating wind turbine using SiL hybrid method, Journal of Physics: Conference Series, 1618, 032 048, https://doi.org/10.1088/1742-6596/1618/3/032048, https://dx.doi.org/10.1088/1742-6596/1618/3/032048, 2020.

Robertson, A., Bergua, R., Fontanella, A., and Jonkman, J.: OC6 Phase III Definition Document, https://doi.org/10.2172/1957538, https://www.osti.gov/biblio/1957538, 2023.

Robertson, A. N., Jonkman, J. M., Goupee, A. J., Coulling, A. J., Prowell, I., Browning, J., Masciola, M. D., and Molta, P.: Summary of Conclusions and Recommendations Drawn From the DeepCwind Scaled Floating Offshore Wind System Test Campaign, Volume 8: Ocean Renewable Energy, https://doi.org/10.1115/OMAE2013-10817, https://doi.org/10.1115/OMAE2013-10817, v008T09A053, 2013.

Sebastian, T. and Lackner, M.: Characterization of the unsteady aerodynamics of offshore floating wind turbines, Wind Energy, 16, 339–352, https://doi.org/https://doi.org/10.1002/we.545, https://onlinelibrary.wiley.com/doi/abs/10.1002/we.545, 2013.

Snel, H. and Schepers, J. G.: Joint investigation of dynamic inflow effects and implementation of an engineering method, 1995.

STEP4WIND: STEP4WIND project, https://step4wind.eu, accessed: 2023-03-19.

Thys, M., Souza, C., Sauder, T., Fonseca, N., Berthelsen, P. A., Engebretsen, E., and Haslum, H.: Experimental Investigation of the Coupling Between Aero- and Hydrodynamical Loads On A 12 MW Semi-Submersible Floating Wind Turbine, Volume 9: Ocean Renewable Energy, https://doi.org/10.1115/OMAE2021-62980, https://doi.org/10.1115/OMAE2021-62980, v009T09A030, 2021.

van der Veen, G. J., Couchman, I. J., and Bowyer, R. O.: Control of floating wind turbines, in: 2012 American Control Conference (ACC), pp. 3148–3153, https://doi.org/10.1109/ACC.2012.6315120, 2012.

Vittori, F., Azcona, J., Eguinoa, I., Pires, O., Rodríguez, A., Morató, A., Garrido, C., and Desmond, C.: Model tests of a 10 MW semi-submersible floating wind turbine under waves and wind using hybrid method to integrate the rotor thrust and moments, Wind Energy Science, 7, 2149–2161, https://doi.org/10.5194/wes-7-2149-2022, https://wes.copernicus.org/articles/7/2149/2022/, 2022.

Yu, W., Lemmer, F., Bredmose, H., Borg, M., Pegalajar-Jurado, A., Mikkelsen, R., Larsen, T. S., Fjelstrup, T., Lomholt, A., Boehm, L., Schlipf, D., Armendariz, J. A., and Cheng, P.: The Triple Spar Campaign: Implementation and Test of a Blade Pitch Controller on a Scaled Floating Wind Turbine Model, Energy Procedia, 137, 323–338, https://doi.org/https://doi.org/10.1016/j.egypro.2017.10.357, https://www.sciencedirect.com/science/article/pii/S1876610217353262, 14th Deep Sea Offshore Wind R&D Conference, EERA DeepWind 2017, 2017.